RSC Advances

PAPER

View Article Online
View Journal | View Issue

Check for updates

Cite this: *RSC Adv.*, 2025, **15**, 8999

Adsorption properties of Merrifield-*bCCA* chelating resins: a new alternative for Pb^{2+} removal from water†

José García-Elías,[a] Adrián Ochoa-Terán, *[a] Eduardo A. López-Maldonado,*[b] Sergio Pérez-Sicairos,[a] Balter Trujillo-Navarrete, [a] Ignacio A. Rivero,[a] Arturo Zizumbo-López, [a] Marisela Martínez-Quiroz[c] and Sandy D. Ramírez-Zatarain[d]

In this work, five new chelating resins (MR_nBz) functionalized with *N*-benzyl bis(carbamoyl)carboxylic acid molecules (Bz*bCCA*) on their surface were prepared to study the metal ion (M^{n+}) adsorption properties in water. MR_nBz resins were characterized by FTIR, TGA, FESEM and EDS. The surface charge as a function of pH and the chemical adsorption of M^{n+} on the surface were evaluated through zeta potential (ζ) measurements. The M^{n+} adsorption capacity of MR_nBz resins was evaluated using Pb^{2+}, Cu^{2+}, Cd^{2+}, and Ni^{2+} mixture model solutions at low concentrations. MR_nBz resins displayed selective adsorption of Pb^{2+} even in the presence of a molar excess of other cations, due to the intrinsic affinity and selectivity of Bz*bCCA* molecules for this metal ion. The adsorption isotherms of Pb^{2+} showed that the adsorption capacity of MR_nBz resins was influenced by the spacer chain length. In addition, the resins were characterized by FTIR, TGA, FESEM and EDS after the M^{n+} adsorption process, confirming the M^{n+} loading on the resin surface.

Received 25th September 2024
Accepted 6th March 2025

DOI: 10.1039/d4ra06929c

rsc.li/rsc-advances

Open Access Article. Published on 24 March 2025. Downloaded on 2/10/2026 6:33:01 PM.
This article is licensed under a Creative Commons Attribution-NonCommercial 3.0 Unported Licence.

1. Introduction

Heavy metal pollution in water has increased dramatically due to its direct association with the growth of industrial activities, such as electroplating, batteries, pesticides, mining, rayon production, metal rinsing processes, tanning, fluidized bed bioreactors, textiles, metal casting, petrochemicals, paper manufacturing and electrolysis applications.[1] This has caused serious damage to the environment and the organisms in ecosystems, as heavy metals are toxic, non-biodegradable and lead to bioaccumulation, posing a risk to human health.[2,3] Each country establishes specific regulations and national or international standards that regulate the permissible concentration limits of heavy metals in aqueous systems, such as the EPA (Environmental Protection Agency) in the USA and SEMARNAT (Secretaría del Medio Ambiente y Recursos Naturales) in Mexico.[4] Heavy metals are considered chemical elements with high density (greater than 5 g cm^{-3}), with mass and atomic weight above 20 units, and they are toxic even in low concentrations. Some of these elements include aluminum (Al), beryllium (Be), copper (Cu), iron (Fe), manganese (Mn), cadmium (Cd), mercury (Hg), and lead (Pb), among others.[5–7] In Mexico, the Official Mexican Standard NOM-001-SEMARNAT-2021 establishes the maximum permissible limits for on-site measurements of Pb^{2+} (2.0 mg L^{-1}), Cd^{2+} (1.0 mg L^{-1}), Cu^{2+} (20.0 mg L^{-1}) and Ni^{2+} (8.0 mg L^{-1}) in wastewater discharges to sewage systems. These regulations aim to prevent and control the contamination of national waters and resources, as well as protect the infrastructure of these systems.[8]

There are various processes for heavy metal treatment (physical-chemical techniques), such as chemical precipitation, coagulation–flocculation, flotation, membrane filtration (ultrafiltration, nanofiltration, reverse osmosis), ion exchange, electrochemical treatment techniques (electrodialysis, membrane electrolysis, electrochemical precipitation), adsorption and the use of biomass and microbial processes, which have proven to be of interest.[9]

Compared with other methods, adsorption processes are the most widely used due to their low operating cost, high adsorption capacities, reusability, and high efficiency in removing various contaminants.[10] Among the most common functional chemical groups used to achieve adsorption properties are oxygen (alcohols, crown ethers) and nitrogen (amines, amides) donors, which have proven to be the most effective for

[a]*Centro de Graduados e Investigación en Química, Tecnológico Nacional de México/IT de Tijuana, Tijuana, B. C., Mexico. E-mail: adrian.ochoa@tectijuana.edu.mx*
[b]*Facultad de Ciencias Químicas e Ingeniería, Universidad Autónoma de Baja California, Tijuana, B. C., Mexico. E-mail: elopez92@uabc.edu.mx*
[c]*CETYS Universidad, Tijuana, B. C., Mexico*
[d]*Departamento de Ingeniería Química y Bioquímica, Tecnológico Nacional de México/IT de Tijuana, Tijuana, B. C., Mexico*

† Electronic supplementary information (ESI) available. See DOI: https://doi.org/10.1039/d4ra06929c

© 2025 The Author(s). Published by the Royal Society of Chemistry

Open Access Article. Published on 24 March 2025. Downloaded on 2/10/2026 6:33:01 PM. This article is licensed under a Creative Commons Attribution-NonCommercial 3.0 Unported Licence.

achieving efficient adsorption.[11] Several natural and synthetic adsorbents have been tested for removing contaminants from aqueous media.[12–19] Chelating resins containing ionizable residues (carboxylic, phosphonic and sulfonic acids) have also proved to be very useful in the treatment of heavy metals.[20]

Considering the increase in environmental awareness, both academia and industry have focused enormous efforts to develop more efficient and selective methods in chemical processes. The Merrifield's resin was introduced in 1963 as a solid support for peptide synthesis,[21] but different modifications have been performed for various purposes.[22–27] The synthesis of carbamates using chelated iron supported on organic molecules has also been reported.[28] Various synthetic strategies were used to modulate the selectivity of reducing agents, such as varying the interconnection chain length of alkyldiamines in the reduction of imines for the formation of chelating amines.[29] Modified resins are useful synthetic platforms because these materials are easily recovered by filtration. Therefore, they can be reused instead of been disposed as waste.[30]

On the other hand, the anchoring of the flavonoid morin to the Merrifield's resin gave the formation of morin-metal complexes in the removal of metals from an aqueous solution.[31] Chemo-sorbents based on porous materials treated with amines have also gained attention recently due to their numerous basic sites that can interact with acidic SO_2.[32] Furthermore, the covalent bonding of Merrifield's resin with primary, secondary and tertiary amines allowed for SO_2 adsorption at low concentration.[33] The support of chelating compounds such as heterofluorenone[34] and tri-pyridine aniline[35] on Merrifield's resin was achieved with the aim of capturing metal cations such as Cu^{2+}, Pb^{2+} and Ni^{2+} from aqueous solutions. A supported dithiocarbamate has been used for the determination of Pb^{2+} in samples of contaminated aqueous effluents and soils, demonstrating the reusability capacity of the functionalized resin for up to 100 cycles.[36] The removal of transition metal ions was reported with supported calix[4]arene-type ligands,[37–39] showing the best removal results with Pb^{2+} and Cr^{6+} ions. Supported bis(azoimidazole) ligands[40] were efficient in the removal of Cu^{2+} and Ag^{+}. Furthermore, supported quercetin was efficient in the removal of Pb^{2+}.[41,42] Lanthanide ions such as Eu^{3+} have also been removed using supporting calix[4]arene-tetraphosphonate chelating resins.[43] Polymeric resins based on Merrifield's resin grafted with polyvinyltetrazol have also been used in the removal of Pb^{2+}, Ni^{2+} and Cu^{2+}.[44] Natural products such as chitosan have been supported in Merrifield's resin and used to remove Cu^{2+}.[45] Some chelating resins with dual adsorption capability for a variety of cations were prepared, simultaneously supporting glycidylmethacrylate, 5-aminosalicylicacid and 2-(4-imidazolyl)ethylamine, and evaluated in the removal of harmful metals, such as Cu^{2+} and Pb^{2+}, Fe^{3+} and Cr^{3+}, as well as Cd^{2+} and Ag^{+}.[46]

The design of new compounds with low structural complexity for the detection and removal of metal ions has attracted attention in the area of environmental chemistry due to the biological and environmental importance of metal ions. One example is the bis(carbamoylcarboxylic) acids (*bCCA*s), which have been studied as chelating agents for metal ions to achieve the formation of complexes in organic and aqueous media.[47,48] Previously, it was reported by Lingaiah *et al.* that monotopic carbamoylcarboxylic acids form coordination complexes with metal ions such as Cu^{2+} through a metal-heteroatom ionic bond with the carboxylate group and a coordination bond with the amide carbonyl group.[49] On the other hand, *N*,*N*-dibenzyl, *N*,*N*-dinaphthyl and *N*,*N*-dinaphthylmethyl *bCCA*s interact with Pb^{2+}, Cu^{2+}, Hg^{2+} at specific 1 : 1 ligand–metal ratios. It is noteworthy that Pb^{2+} complexes precipitate in aqueous media, reaching removal efficiencies up to 95% and an average removal capacity of 3.3 mg of Pb^{2+}/mg of ligand at pH 2.5.[50] The simultaneous removal of seven metal ions was also achieved with aniline- and pyridine-functionalized *bCCA*s, showing good average removal efficiencies and capacities of 1.08 to 19.3 mg of M^{n+}/mg of ligand at pH 4.0.[51] Due to the ditopic nature of *bCCAs*, the formation of coordination

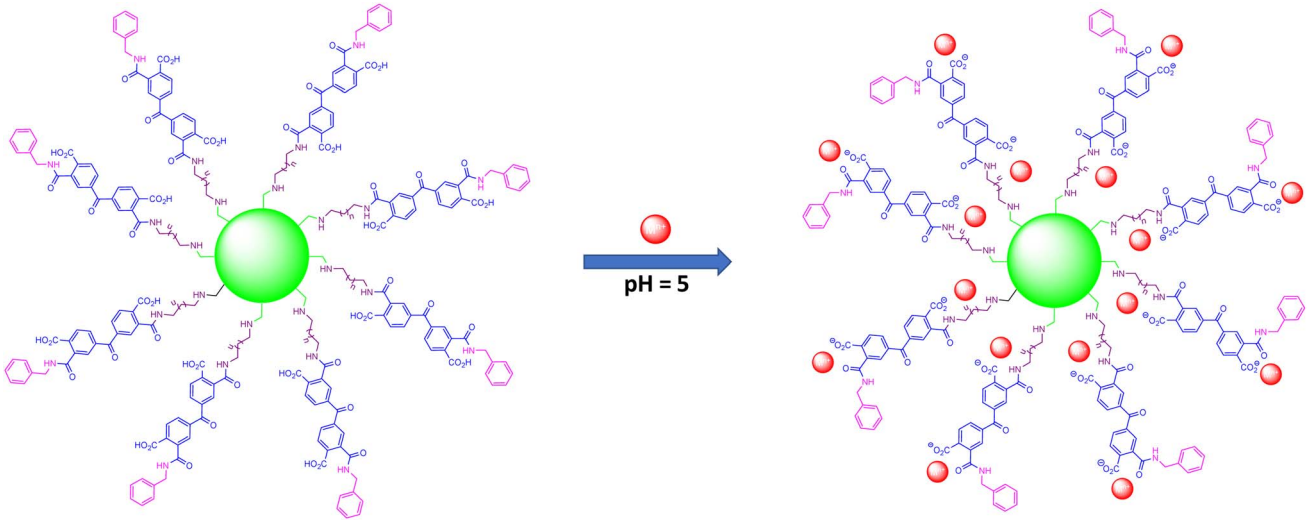

Fig. 1 Merrifield-*bCCA* (MR_nBz) chelating resins for the removal of metal ions.

© 2025 The Author(s). Published by the Royal Society of Chemistry

Open Access Article. Published on 24 March 2025. Downloaded on 2/10/2026 6:33:01 PM. This article is licensed under a Creative Commons Attribution-NonCommercial 3.0 Unported Licence.

polymers or aggregates with these ligands has been proposed. Once the precipitates are formed in the aqueous medium, the cations are separated from water.

Furthermore, chitosan grafted with *N*-benzyl *bCCA* achieved the simultaneous removal of a mixture of cations with good efficiency (66% to 99%),[52] but a high dose of grafted polymer was required (1.12 to 1.15 mg of M^{n+}/mg of grafted chitosan). The performance parameters were improved by grafting the chitosan with aniline- and pyridine-functionalized *bCCA*s. The grafted chitosan showed good removal efficiencies (73% to 99%) and excellent removal capacities of metal ions (43.5 to 50 mg of M^{n+}/mg of grafted chitosan) at pH 4.4.[53]

In this work, we propose the immobilization of the chelating compound *N*-benzyl *mCCA* on the Merrifield's resin to synthetize new Merrifield-*bCCA* chelating resins (**MR$_n$Bz**) in order to study their metal ion adsorption properties and their potential as new alternatives for the removal of Pb^{2+} ions from water, taking advantage of the outstanding *bCCAs* coordination/chelation properties and affinity, as well as the characteristics of Merrifield's resin (Fig. 1). Based on previous reports with this type of ligand, it is proposed that complexation is the main mechanism of cation adsorption on the resin (Fig. 1). These resins have high affinity and selectivity in the adsorption of Pb^{2+} even in the presence of other excess metal cations. Removal efficiencies greater than 90% in a concentration range from 3.5 to 74 mg L^{-1} in the experiments were carried out in batches, and they can also be reused at least four times. All these characteristics demonstrate the potential of these chelating resins for applications in the treatment of wastewater contaminated with metals, particularly lead.

2. Experimental

2.1 Apparatus

Fourier transform infrared spectra were recorded in the frequency range of 400–4000 cm^{-1} using a Perkin FTIR Spectrum Two spectrophotometer. The microstructure of samples was detected by field emission scanning electron microscopy (FESEM), and were carried out with a JEOL 7800 PRIME microscope with a 5 keV electron beam. Zeta potential analysis was conducted using a Meinsberger Zeta Stabino Particle Metrix, GmbH A0207 Titration System instrument and a porcelain cuvette. The thermal stability of the adsorbents was detected through thermogravimetric analysis (TGA), recorded *via* the TA instrument SDT 2960 simultaneous DSC-TGA model by raising the temperature from 30 °C to 800 °C using ceramic pans at a rate of 20 °C min^{-1} under N_2 atmosphere. The metal ion concentration was determined using a PerkinElmer induced coupled plasma atomic emission spectrometer (ICP-AES) Optima 8300 model; the Argon plasma, auxiliary and nebulizer flow were 15.00 L min^{-1}, 0.20 L min^{-1} and 0.55 L min^{-1}, respectively, with a radio frequency of 1300 W and a sample flow rate of 1.5 L min^{-1}.

2.2 Reagents

Merrifield's resin (MR) was used with 200–400 mesh, and the following extent of labeling: 3.5–4.5 mmol g^{-1} of Cl loading, 1% cross-linked. All compounds were purchased from Merck and Sigma companies, and used as received without further purification. All aqueous metal ion solutions were prepared using deionized water.

2.3 Preparation of chelating resins

2.3.1 Preparation of aminoalkyl-functionalized Merrifield's resins (MR$_n$). Merrifield's resin (2.5 g, 10 mmol) was placed into a 250 mL round-bottom flask. It was expanded into 60 mL of THF : DMF (1 : 1), then K_2CO_3 (4.1463 g, 30 mmol) and KI (0.8300 g, 5 mmol) were added. The mixture was stirred in an orbital oscillator shaker for 30 min at 250 rpm, then the corresponding alkyldiamine (30 mmol) was added and the mixture was stirred for 12 h at 250 rpm. Finally, water (30 mL) was added and stirred for 30 min. Then, the product resin was filtered and washed with water (3 × 5 mL), MeOH (3 × 5 mL), THF (3 × 5 mL), DCM (3 × 5 mL) and Et_2O (3 × 5 mL), and dried under vacuum. This procedure was repeated twice to ensure the complete functionalization of the resin.

Merrifield's ethylenediamine resin (**MR$_2$**). 2.65 g, 97% recovery yield. FTIR (ATR): 3300, 3022, 2914, 1447, 695 cm^{-1}. TGA (°C, Δ*w*): 166.9 °C (1.9), 441.3 (81.1), 528.8 (5.5).

Merrifield's propylenediamine resin (**MR$_3$**). 2.75 g, 96% recovery yield. FTIR (ATR): 3289, 3024, 2918, 1450, 700 cm^{-1}. TGA (°C, Δ*w*): 141.2 (3.8), (4.9), 418.2 (71.3), 533.2 (4.6).

Merrifield's butylenediamine resin (**MR$_4$**). 2.83 g, 94% recovery yield. FTIR (ATR): 3290, 3018, 2915, 1445, 694 cm^{-1}. TGA (°C, Δ*w*): 154.43 (0.99), 328.4 (8.8), 444.9 (71.8), 533.6 (4.6).

Merrifield's hexylenediamine resin (**MR$_6$**). 2.93 g, 89% recovery yield. FTIR (ATR): 3308, 3020, 2917, 1449, 697 cm^{-1}. TGA (°C, Δ*w*): 155.3 (0.49), 355.0 (11.5), 446.7 (76.4), 559.9 (8.6).

Merrifield's octylenediamine resin (**MR$_8$**). 2.78 g, 78% recovery yield. FTIR (ATR): 3278, 3020, 2920, 1449, 699 cm^{-1}. TGA (°C, Δ*w*): 151.0 °C (1.8), 366.3 (12.0), 451.9 (79.5).

2.3.2 Preparation of aminoalkyl-carbamoylcarboxylic acid Merrifield's resins (MR$_n$Bz). The corresponding aminoalkyl-functionalized Merrifield's resin (6 mmol) was placed into a 250 mL round-bottom flask under an inert [Ar] atmosphere, then dry DCM (40 mL) was added to expand the resin, and the mixture was stirred for 30 min. The benzophenone-3,3′,4,4′-tetracarboxylic dianhydride (5.80 g, 18 mmol in 20 mL of dry THF) was added *via* cannula, and the mixture was stirred for 6 h at 250 rpm. Then, benzylamine (5.1437 g, 5.24 mL, 48 mmol) was added and the reaction was stirred continuously for 6 h. Finally, 30 mL of water at 50 °C was added to the reaction, and it was stirred for 15 min. The mixture was vacuum filtered and washed with water (3 × 20 mL), MeOH (3 × 20 mL), THF (3 × 20 mL), DCM (3 × 20 mL) and Et_2O (3 × 20 mL). This procedure was repeated twice to insure the complete functionalization of the resin.

Merrifield's ethylenediamine carbamoylcarboxylic acid resin (**MR$_2$Bz**). 2.45 g, 64% recovery yield. FTIR (ATR): 3390, 3022, 2920, 1658, 1603, 1549, 1359, 699 cm^{-1}. TGA (°C, Δ*w*): 189.2 (9.1), 324.5 (3.7), 527.1 (54.4), 570.7 (6.2).

Merrifield's propylenediamine carbamoylcarboxylic acid resin (**MR$_3$Bz**). 2.58 g, 69% recovery yield. FTIR (ATR): 3404,

Open Access Article. Published on 24 March 2025. Downloaded on 2/10/2026 6:33:01 PM. This article is licensed under a Creative Commons Attribution-NonCommercial 3.0 Unported Licence.

3021, 2925, 1773, 1604, 1554, 1357, 696 cm^{-1}. TGA (°C, Δw): 191 (11.9), 439.1 (53.9), 573.1 (7.2).

Merrifield's butylenediamine carbamoylcarboxylic acid resin (**MR_4Bz**). 2.42 g, 67% recovery yield. FTIR (ATR): 3410, 3022, 2925, 1765, 1645, 1605, 1553, 1355, 696 cm^{-1}. TGA (°C, Δw): 190.0 (8.8), 314.8 (2.4), 444.2 (69.6).

Merrifield's hexylenediamine carbamoylcarboxylic acid resin (**MR_6Bz**). 2.60 g, 75% recovery yield. FTIR (ATR): 3404, 3026, 2922, 1761, 1700, 1558, 1354, 695 cm^{-1}. TGA (°C, Δw): 198.7 (8.5), 323.7 (3.2), 441.1 (58.6), 564.4 (5.2).

Merrifield's octylenediamine carbamoylcarboxylic acid resin (**MR_8Bz**). 2.13 g, 65% recovery yield. FTIR (ATR): 3370, 3026, 2923, 1769, 1708, 1563, 1354, 697 cm^{-1}. TGA (°C, Δw): 201.0 (9.6), 446.2 (74.9).

2.4 Zeta potential measurements

For the measurements of the ζ variation as function of pH, 20 mg of a chelating resin was suspended in 10 mL of deionized water. Then, 200 μL of a 1.1 M HCl solution was added, and the suspension was obtained at a final volume of 20 mL. The initial pH was around 2.3. Then, 20 μL aliquots of a 0.1 M NaOH solution were added, and the changes in pH and ζ were registered.

The measurements of the ζ variations as a function of M^{n+} concentration were performed using 20 mg of a different chelate resin in 20 mL of deionized water, adjusting the pH at 5.0 with a 0.1 M HCl solution. Each material was titrated with a single metal ion solution at 0.16 M (Cu^{2+}, Pb^{2+}, Ni^{2+} and Cd^{2+}), adding 10 μL aliquots until the isoelectric point was reached or the ζ potential value remained constant.

2.5 Metal ion adsorption of chelating resins MR_nBz

The metal removal test was performed using a batch modified micro jar technique with a $Pb(NO_3)_2$ solution at 28.2 mg L^{-1} of Pb^{2+}. The dosage tests were carried out in 10 mL of metal solution with the addition of a progressive addition of 10, 20, 30, 40 and 50 mg of the chelating resin to the solution. The vials were shaken for 1 h, and allowed to stand before being filtered. Finally, the supernatant was evaluated to determine the residual concentration of the metal using the ICP-IOEs atomic emission technique. Three parallel experiments were performed, and the final concentration values correspond to the average of the three measurements.

A second metal removal test was performed using a batch modified micro jar technique with $Ni(NO_3)_2$, $Pb(NO_3)_2$, $Cd(NO_3)_2$ and $Cu(NO_3)_2$, equivalent to 23.75 mg L^{-1} of Ni^{2+}, 33.51 mg L^{-1} of Pb^{2+}, 21.46 mg L^{-1} of Cd^{2+} and 27.49 mg L^{-1} of Cu^{2+}. The dosage tests were carried out in 10 mL of metal solution with the progressive addition of 10, 20, 30, 40 and 50 mg of the chelating resin to the solution. The vials were shaken for 1 h, and allowed to stand to be filtered. Finally, the supernatant was evaluated to determine the residual concentration of the metal using the ICP-IOEs atomic emission technique. Three parallel experiments were performed, and the final concentration values correspond to the average of the three measurements.

The removal percentage, E (%), was calculated using eqn (1):

$$E(\%) = \frac{C_i - C_F}{C_i} \times 100 \quad (1)$$

where: C_i = initial concentration of metal ion (mg L^{-1}). C_f= final concentration of metal ion (mg L^{-1}).

2.6 Equilibrium binding experiments for the study of metal adsorption isotherms

For the adsorption isotherms, 10 mg of **MR_nBz** ($n = 3, 4, 6$) were dispersed in 10 mL of a Pb^{2+} solutions at different concentrations (20 to 423 mg L^{-1}). The mixture was kept in contact for 1 h to ensure adsorption equilibrium. Then, the **MR_nBz** resins were separated from the solution by filtration. The amount of Pb^{2+} adsorbed onto the resins was determined by the difference between the initial Pb^{2+} concentration and the concentration remaining in the supernatant. Three parallel experiments were performed, and the final concentration values correspond to the average of the three measurements.

The equilibrium adsorption amounts of Pb^{2+} were calculated according to eqn (2):[54]

$$Q_e = \frac{(C_0 - C_e)V}{m} \quad (2)$$

where Q_e (mg g^{-1}) is the amount of Pb^{2+} adsorbed at equilibrium, C_0 and C_e (mg L^{-1}) are the concentrations of Pb^{2+} at the initial state and equilibrium, respectively, V is the volume of Pb^{2+} solution, and m is the mass of the resin.

3. Results and discussion

3.1 Synthesis and characterization of the Merrifield-bCCA chelating resins

Five Merrifield-*bCCA* chelating resins **MR_nBz** were prepared using Merrifield's resin (**MR**) as the starting material (Scheme 1). **MR** was selected due to its robustness and chemical resistance in acidic media. Furthermore, it does not expand in water, so its separation by filtration is quick and simple.[55] It was proposed to immobilize the compound *N*-benzyl-*bCCA* because the free *N*,*N*′-dibenzyl-*bCCA* has a great affinity towards Pb^{2+}, and exerts selective and efficient removal at low pH. Then, **MR** resin was reacted with five different length alkyldiamines in order to introduce the required amino-functionality to support the chelating molecule, as well as a spacer between the polymer matrix and the *bCCA* molecule. The amino-functionalized Merrifield's resins **MR_n** were obtained with good recovery yields (78% to 97%). Then, the benzophenone-3,3′,4,4′-tetracarboxylic dianhydride reacted with the **MR_n** resins to form a mono-carbamoylcarboxylic acid supported on solid phase through the reaction of the amino-resin group with one anhydride of the reactant. Then, benzylamine (**Bz**) was added *in situ* to react with the available anhydride group, forming the corresponding *bCCA* molecule supported on the polymer. **MR_nBz** chelating resins were obtained in 64 to 75% recovery yields.

3.1.1 FTIR characterization. Fig. 2a shows the FTIR spectra for Merrifield's resin and the resins obtained in each synthetic step. The spectrum of **MR** (red) has the characteristic bending

 © 2025 The Author(s). Published by the Royal Society of Chemistry

Open Access Article. Published on 24 March 2025. Downloaded on 2/10/2026 6:33:01 PM.
This article is licensed under a Creative Commons Attribution-NonCommercial 3.0 Unported Licence.

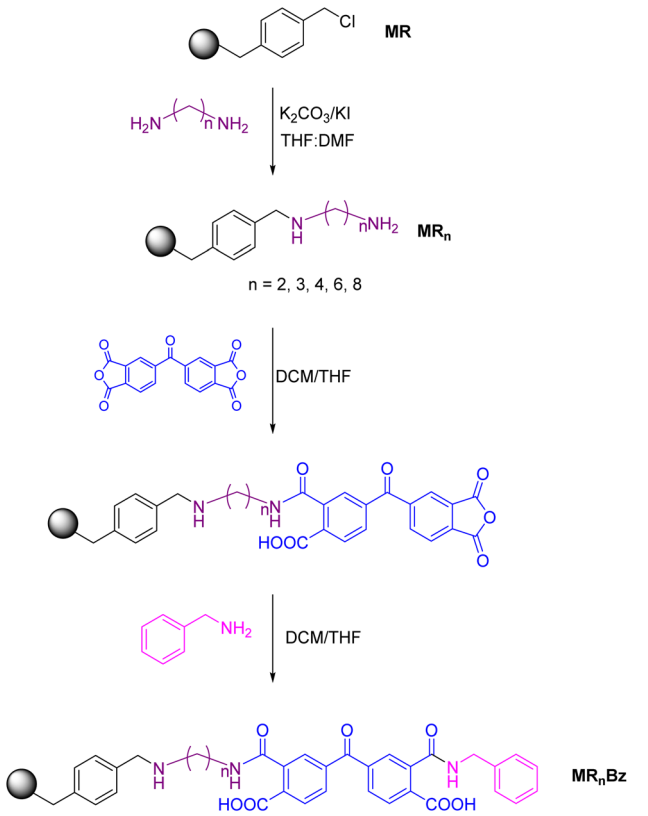

Scheme 1 Synthetic route for the chelating Merrifield-*bCCA* (MR_nBz) resins.

vibration at 1262 cm^{-1} of the methylene group linked to chlorine and the vibration at 662 cm^{-1} corresponding to the carbon–chlorine bond stretching. The spectrum of the aminoalkyl-functionalized **MR_4** resin (blue) does not show the vibrations at 1262 and 662 cm^{-1}, indicating that the substitution of chlorine in the resin by the diamines was successful. Finally, in the IR spectrum of **MR_4Bz** resin (magenta), a peak is observed at 3453 cm^{-1} that corresponds to the amide N–H bond stretching, and a wide band extending up to 2400 cm^{-1} corresponds to the O–H bonds of the carboxylic acids. From 1800 to 1650 cm^{-1}, a series of vibrations corresponding to carbonyl groups are also observed. These vibrations confirm the presence of the *N*-benzyl-*bCCA* molecule attached to the polymer resin. Fig. 2b compares the spectra of the **MR_4Bz** chelating resin with the free *N*,*N*-dibenzyl carbamoylcarboxylic acid (***b*BzCCA**). It is observed that when the vibrational bands at 1738, 1724 and 1657 cm^{-1} of the free *bCCA* are weaker than that expected for a common carbonyl group, then the vibrations observed in the chelating resin are also weak. Similar results were obtained in the FTIR characterization of the rest of the prepared resins (Fig. S1 to S4†).

3.1.2 Thermogravimetric analysis. The thermogravimetric analysis of the **MR**, **MR_n** and **MR_nBz** resins was performed at 20 °C min^{-1} under a nitrogen atmosphere (Fig. 3 and S5–S8†). The thermogram of **MR** (red) shows three thermal weight loss events; the first occurs at a maximum temperature of 331.7 °C with a weight loss of 16.55%, which may be attributed to the

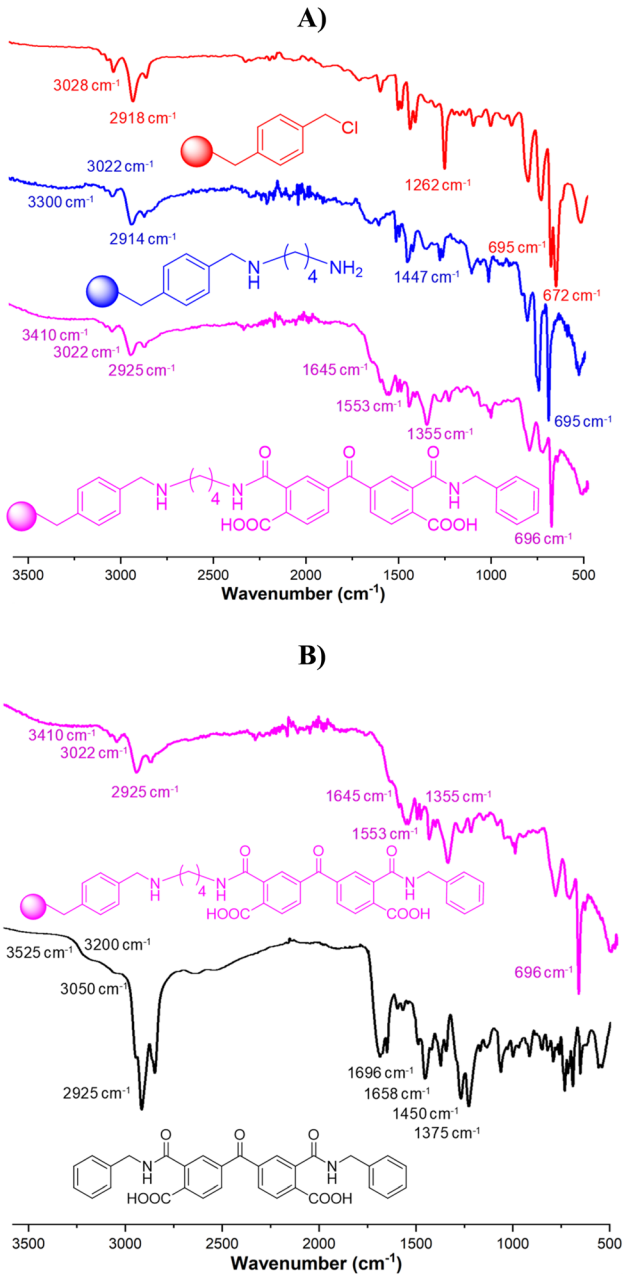

Fig. 2 (A) FTIR spectra of Merrifield's resin (red), MR_4 resin (blue) and MR_4Bz (magenta). (B) FTIR spectra of MR_4Bz (magenta) and BzCCA (black).

pyrolysis of the chloromethylene group. Chlorine has a molar mass of 35.45 g mol^{-1} and corresponds theoretically to the 14.18% of Merrifield's resin mass, considering the average load of 4.0 mmol of Cl reported by the supplier. Based on these results, a loading of 4.72 mmol of Cl/g of resin was calculated from the experimental data. The second weight loss event is held at 459 °C with a weight loss of 43.48%. The last event occurs at 526.5 °C, having a weight loss of 14.00%, and the final residue was 23.20%. The thermogram of **MR_4** resin (blue) shows a noticeable change in the thermal decomposition pattern. The thermal event in **MR** at 331.7 °C is not observed in this resin, confirming the substitution of chlorine by the alkyldiamine.

Open Access Article. Published on 24 March 2025. Downloaded on 2/10/2026 6:33:01 PM.
This article is licensed under a Creative Commons Attribution-NonCommercial 3.0 Unported Licence.

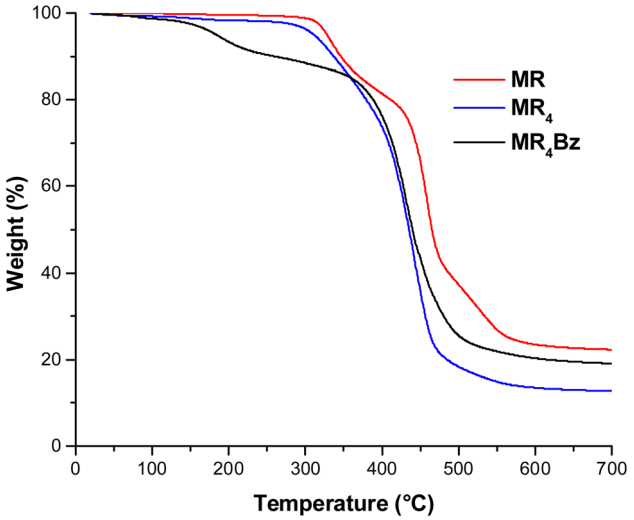

Fig. 3 Thermograms of Merrifield's resin (red), MR_4 resin (blue) and MR_4**Bz** resin (black) obtained at 20 °C min^{-1} under a N_2 atmosphere.

The first thermal event corresponds to a weight loss of 8.85% at 328 °C. The second event was found at 444 °C with a weight loss of 71.8%. The third thermal event occurs at 533.5 °C with a weight loss of 4.59%. Finally, the residue of this functionalized resin was 8.15%. These results indicate that the functionalization of the resin with the alkylenediamine changes its thermal properties.

Finally, the thermogram of the chelating resin **MR_4Bz** (black) shows three main thermal decomposition events. The first thermal event is observed at 190.0 °C with a weight loss of 8.83%. The second event with a weight loss of 2.40% occurs at a temperature of 314 °C, and the third event is observed at 445 °C with a 69.68% weight loss.

The thermogravimetric analysis of the free mono- and bis(-carbamoylcarboxylic) acids, ***m*BzCCA** and ***b*BzCCA**, was useful in the interpretation of the thermal properties of the chelating resins (Fig. 4, S9 and S10†). These compounds present two well defined thermal events, the first at 187.6 °C and 193.0 °C, which corresponds to a weight loss of 13.5% and 16.12%, respectively. These events are attributed to the pyrolysis of one and two carboxylic acids present in their molecules, since they theoretically represent 10.2% and 16.4% of their molecular weight. The second thermal event occurs at 470.6 °C and 490.0 °C with 72.98% and 74.82% weight losses, respectively, corresponding to the thermal decomposition of the rest of the molecule.

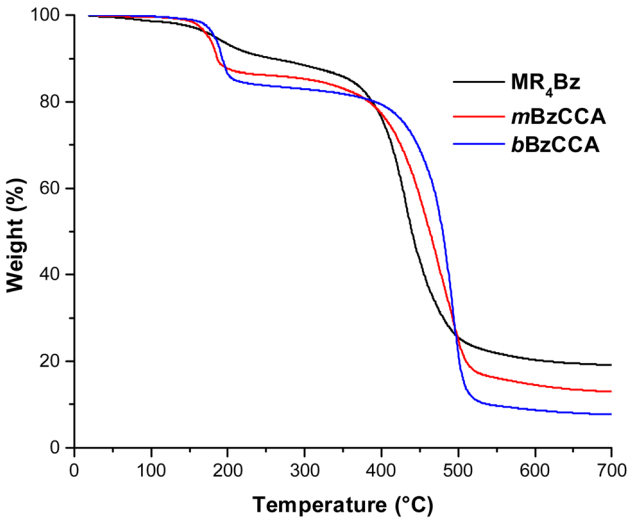

Fig. 4 Thermograms of MR_4**Bz** resin (black), ***m*BzCCA** (red) and ***b*BzCCA** (blue) obtained at 20 °C min^{-1} under a N_2 atmosphere.

It can be seen that the thermogram of the chelating resin **MR_4Bz** also presents a thermal event at 190 °C, which by comparison may be attributed to pyrolysis of the carboxylic acid groups in the molecules attached to the polymer resin. Based on the weight loss of this thermal event, a loading of 1.00 mmol of *bCCA*/g of resin was calculated, which agrees with the theoretical calculated loading of 1.37 mmol of *bCCA*/g of resin. The thermograms for the other **MR_nBz** resins show the same thermal event (Fig. S11 to S14†), and the calculated loading values were 1.03 mmol g^{-1} for **MR_2Bz**, 1.35 mmol g^{-1} for **MR_3Bz**, 0.97 mmol g^{-1} for **MR_6Bz** and 1.09 mmol g^{-1} for **MR_8Bz**.

3.1.3 Morphology and elemental analysis of the chelating resins by FESEM and EDS. The morphology of the **MR** and **MR_nBz** resins was observed by FESEM for multiple beads (Fig. 5). As expected, the FESEM images of the **MR** resin show a smooth and flat microsphere surface (A), which is maintained after its functionalization with the alkylenediamines and the *bCCA* (B). It can be clearly observed in the magnification (C) that the resin beads preserve their surface, size and spherical shape along the synthesis steps. The morphological characteristics observed in these materials were like those reported for other polystyrene supported ligands.[56] For its part, the elemental analysis by energy dispersion spectroscopy (EDS) of **MR** shows the presence of carbon. However, in the functionalized resins **MR_3Bz** and **MR_6Bz**, nitrogen and oxygen also are detected, which are present in the alkylenediamine spacer chains and the *b*CCA molecules (Fig. S15–S17†).

3.2 Surface analysis of chelating resins by ζ

Zeta potential measurements were performed to qualitatively and quantitatively analyze the interaction of the free *bCCAs* and *bCCA*-functionalized chitosan with metal ions, and to determinate the affinity and metal ion removal capacity of these materials in a homogeneous phase.[41–44] Then, ζ measurements were performed to investigate the suitability of this technique to analyze the surface chemistry of the chelating resins and the adsorption of metal ions in the heterogeneous phase. Subsequently, the effect of pH over ζ in the resins **MR**, **MR_n** and **MR_nBz** was investigated, suspending 20 mg of each resin in 20 mL of deionized water. The variation of ζ with respect to the pH of pure water was evaluated to determine the existence of a background response. Fig. 6 shows that water gives a background response with an electropositive character at low pH in the range of 2.5 to 5.2 (IEP of water). Subsequently, it becomes electronegative, reaching a limit of ζ (≈ −12 mV) at a pH of 6. The **MR** resin shows a ζ profile similar to water at low pH (2.5 to 4). It then decreases, having an IEP at 4.5 until it reaches an

© 2025 The Author(s). Published by the Royal Society of Chemistry

Open Access Article. Published on 24 March 2025. Downloaded on 2/10/2026 6:33:01 PM.
This article is licensed under a Creative Commons Attribution-NonCommercial 3.0 Unported Licence.

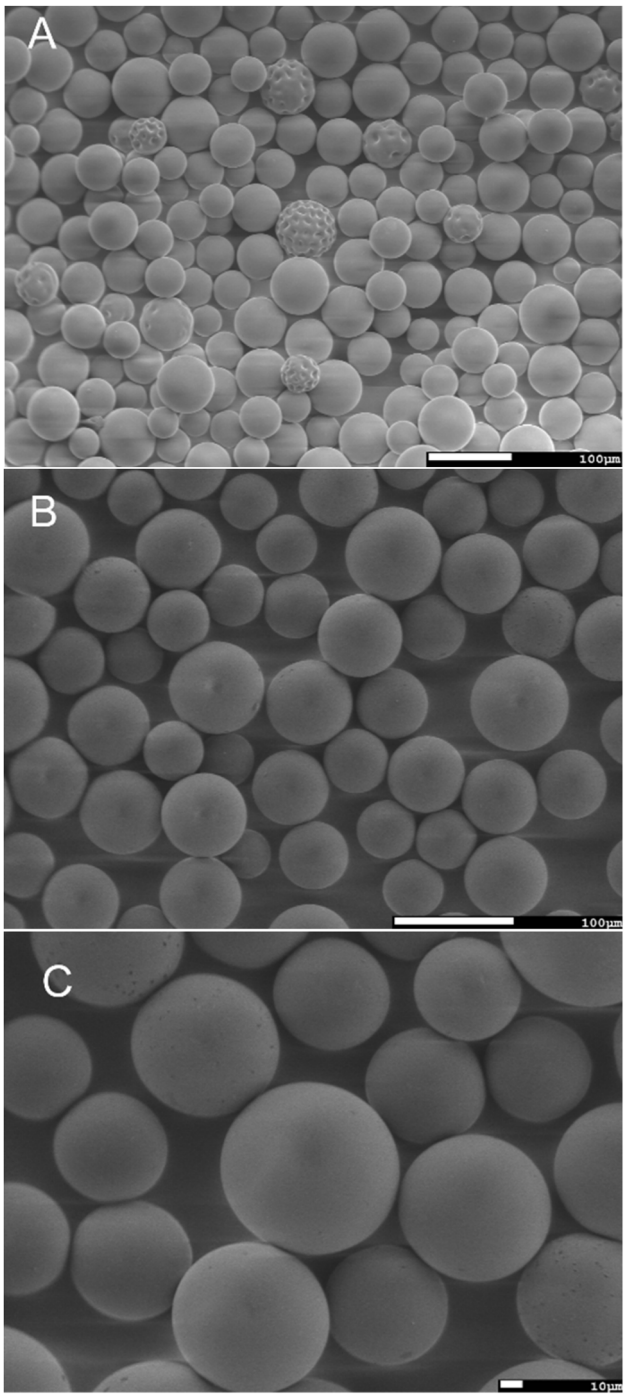

Fig. 5 FESEM images of Merrifield's resin (**MR**) (A) and **MR$_3$Bz** resin (B and C).

electronegative limit of −39.6 mV at pH 6.2. These differences in the response profile with respect to water validate that the zeta potential measurement corresponds to the surface of the resin particles. In general, the shape of the ζ profiles obtained with the **MR$_n$** and **MR$_n$Bz** resins is similar to that of the **MR** resin, with differences in IEPs and ζ limits caused by the chemical modifications on the resin surface (Fig. S18–S20†). For example, the amino-functionalized resin **MR$_3$** presents a maximum ζ limit (ζ_{max}) of 36.6 mV, a minimum ζ limit (ζ_{min}) of −44.0 mV and IEP at 4.65, while *bCCA*-functionalized resin **MR$_3$Bz** has a ζ_{max} of 25.5 mV, a ζ_{min} of −42.8 mV and IEP at 4.05 (Fig. 6A). The same effect is observed in **MR$_6$**, which presents a ζ_{max} of 34.6 mV, a ζ_{min} of −45.2 mV and IEP at 5.02, but the **MR$_6$Bz** resin has ζ_{max} of 21.1 mV, a ζ_{min} of −44.4 mV and IEP at 3.91 (Fig. 6B). As can be seen in Table 1, the most notable change in zeta potential between **MR$_n$** and **MR$_n$Bz** resins occurs in the ζ_{max} at low pH, which becomes more negative. The free ***b*BzCCA** has a negative ζ at low pH. The IEP for this ligand is observed at 2.5, and then the binding of this ligand to the resins causes a decrease in the ζ_{max} at low pH. Also, a slight increase in the IEP of the **MR$_n$** resins with respect to **MR** is observed, in addition to a slight decrease in the **MR$_n$Bz** resins with respect to **MR$_n$**. The IEP corresponds to the pH at which the surface of the resins is neutral, and it is proposed that the negative potential at a pH value higher than the IEP is given by the formation of negative charges on the surface, in this case given by the deprotonation of the carboxylic groups of the *bCCA* molecules that are anchored to the resin (Fig. 6C).

3.3 Surface analysis of chelating resins in the adsorption of metal ions by ζ

Once the superficial characteristics of the **MR$_n$Bz** chelating resins were analyzed by ζ, the effect of the adsorption of metal ions over ζ was evaluated as an indicator of the chemical interaction with the chelating molecules on the resin surface. For these experiments, 10 mg of chelating resin was suspended in 20 mL of deionized water at pH 5.0 into a zeta potential cell, then aliquots of individual metal ion (Pb^{2+}, Cu^{2+}, Cd^{2+} and Ni^{2+}) solutions (0.16 M) were automatically added to the suspension, and the ζ changes were registered. At this pH, the resin surface has a negative surface charge, as indicated in Fig. 6. The ζ study of the **MR$_n$Bz** resins provided stable measurements with Ni^{2+} and Pb^{2+} metal ions in the **MR$_3$Bz** resin and with Pb^{2+} in **MR$_6$Bz** and no other metal ions. Fig. 7 shows that in **MR$_3$Bz** (A) and **MR$_6$Bz** (B) resins, the ζ increases dramatically in the range of 0 to 0.001 M (0.010 mmol) of added Pb^{2+}, which agrees with the calculated *bCCA* loading on resins by TGA, 0.0097 and 0.0109 mmol, respectively. The IEP is reached in both resins with Pb^{2+}, indicating that these resins have great affinity towards this metal ion by the *bCCA* functionalization. In addition, the titrations of the **MR$_3$Bz** resin with Pb^{2+} and Ni^{2+} begin at similar potential limits but different profiles are observed, indicating that the response depends on the affinity towards the metal ion. The rest of the **MR$_n$Bz** resins have a similar behavior with some of the metal ions (Fig. S21–S23†).

An additional experiment was performed to evaluate the ζ response by titrating with a solution containing a mixture of Pb^{2+}, Ni^{2+}, Cd^{2+} and Cu^{2+} in order to determine differences according to their chemical structure at the surface. As can be seen in Fig. 8, the ζ of the ***b*BzCCA** ligand increases with the concentration of M^{n+} due to the metal–ligand interaction,[41] but it does not reach the IEP. On the other hand, the surface of the **MR** resin is not only susceptible to pH, but also to the metal ions present in the solution and the ζ increases gradually with

Open Access Article. Published on 24 March 2025. Downloaded on 2/10/2026 6:33:01 PM.
This article is licensed under a Creative Commons Attribution-NonCommercial 3.0 Unported Licence.

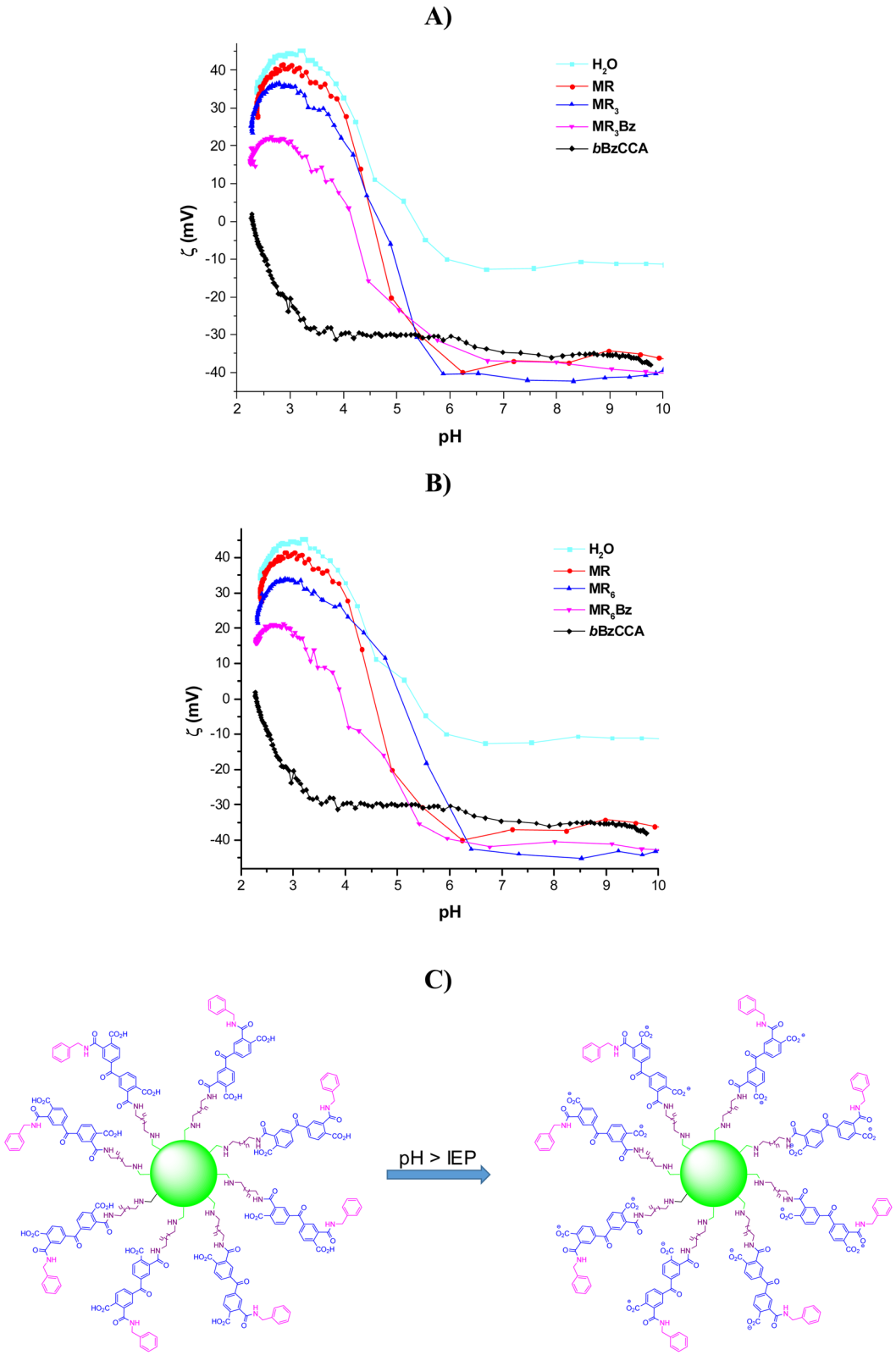

Fig. 6 $\zeta = f[\mathrm{pH}]$ profiles for (A) **MR**, $\mathbf{MR_3}$ and $\mathbf{MR_3Bz}$ and (B) **MR**, $\mathbf{MR_6}$ and $\mathbf{MR_6Bz}$. (C) Schematic of the deprotonation of *bCCA* molecules attached to the resins, forming negative charges. Mass of resin: 20 mg. Volume: 20 mL. Solvent: deionized water.

the M^{n+} concentration, but the IEP is not reached either. Taking the asymptotic profile of ζ for this resin as a basis, it is now observed that by modifying the surface of the resin, the curvature of the asymptote is modified, showing a more abrupt neutralization effect in the amino-functionalized $\mathbf{MR_8}$ resin and even more marked response in the *bCCA*-functionalized $\mathbf{MR_8Bz}$

© 2025 The Author(s). Published by the Royal Society of Chemistry

Open Access Article. Published on 24 March 2025. Downloaded on 2/10/2026 6:33:01 PM. This article is licensed under a Creative Commons Attribution-NonCommercial 3.0 Unported Licence.

Table 1 Zeta potential limits and IEP values for MR, MR_n and MR_nBz resins

Resin	ζ_{max} (mV)	ζ_{min} (mV)	$\Delta\zeta$ (mV)	IEP
MR	41.5	−40.0	81.5	4.54
MR_2	36.9	−39.0	78.9	4.40
MR_2Bz	22.1	−46.2	68.3	4.20
MR_3	36.6	−44.0	80.6	4.65
MR_3Bz	25.5	−42.8	68.3	4.05
MR_4	34.0	−44.3	78.3	4.64
MR_4Bz	23.8	−44.3	68.1	4.42
MR_6	34.6	−45.2	79.8	5.02
MR_6Bz	21.1	−44.4	65.5	3.91
MR_8	33.2	−48.1	81.3	4.69
MR_8Bz	19.5	−35.0	54.5	4.23

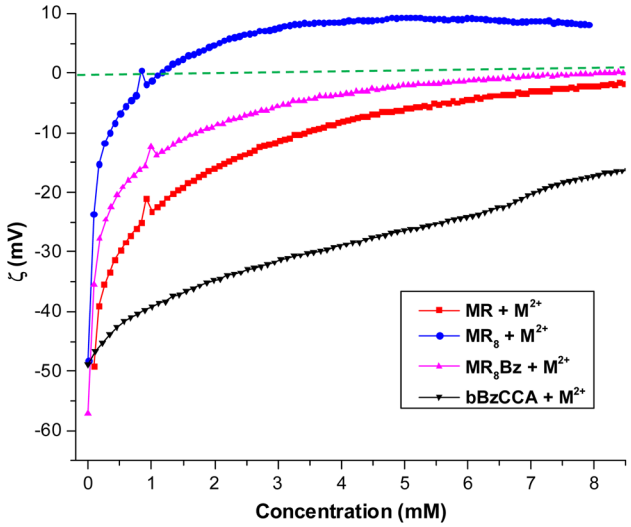

Fig. 8 $\zeta = f[M^{n+}]$ profiles of *b*BzCCA, MR, MR_8 and MR_8Bz obtained by titration with a mixture of metal ions. Mass of resin: 20 mg. Volume: 20 mL. Solvent: deionized water. pH: 5.0.

resin. Also, it is observed that the **MR_8** resin almost reaches the IEP, while **MR_8Bz** exceeds the IEP at low M^{n+} concentration and stabilizes at an electropositive potential. Then, it is more than evident that the *bCCA* molecules attached to the resin enhance the interaction with the metal ions on the resin surface. A similar behavior is observed with the rest of the resins (Fig. S24–S27†).

3.4 Metal ion adsorption in MR_nBz chelating resins

Previous studies have demonstrated that *bCCA*s have a great affinity and removal efficiency over the Pb^{2+} ion.[41,42] Then, the performance of the **MR_nBz** resins was first evaluated using 10 mL of a 28.2 mg Pb^{2+} per L (0.136 mmol L^{-1}) aqueous solution by varying the amount of **MR_nBz** resin at pH 5, in order to find the optimal dose (lower resin amount and maximum cation removal) in the removal of Pb^{2+} from the aqueous solution for 1 h of contact. At this pH, the surface of the resins has a negative character and lead is in the cationic form.[57,58] Table 2 and S28–S32† indicate that the optimal dose of chelating resin under these experimental conditions was 10 mg. The removal% values were greater than 83% and the adsorptions were in the range of 23.4 to 27.4 mg Pb^{2+} per g (0.114 to 0.132 mmol Pb^{2+} per g) under these experimental conditions. Also, beyond this dose, the removal% slightly decreases. This is probably due to a re-dispersion process, which is very common in a coagulation–flocculation process. As seen in Table 3, the final concentration of Pb^{2+} achieved with most of the **MR_nBz** resins is below to the limit allowed by the Official Mexican Standard, meaning that treated water would have the necessary quality for discharge into the municipal sewage system.

Once the optimal resin mass was determined, we proceeded with the optimization of the pH value and contact time. The study of the variation of the Pb^{2+} adsorption of the chelating resins with respect to pH (2.5 to 7.0) shows that the pH value of 5 is precisely optimal for the adsorption of this cation; this is

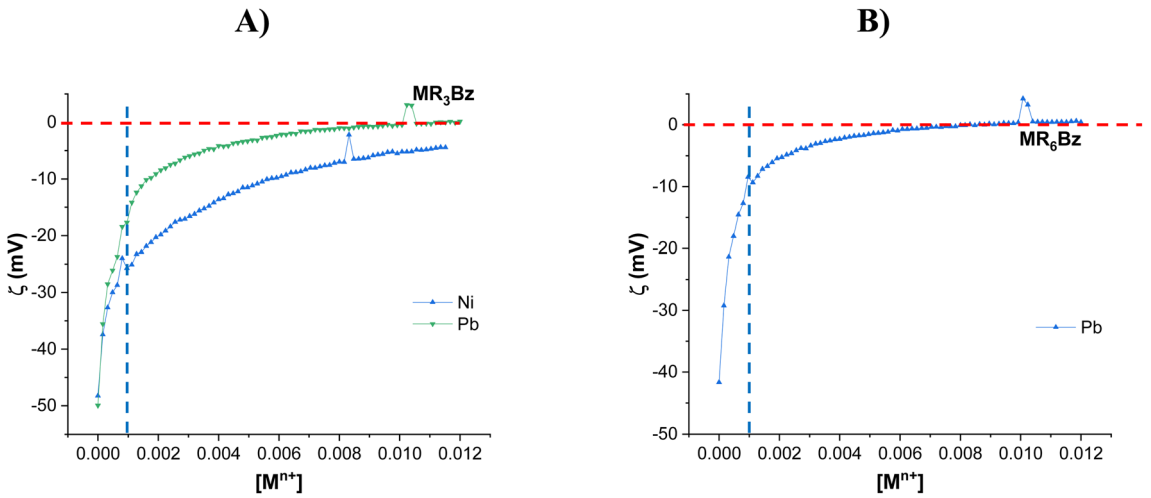

Fig. 7 $\zeta = f[M^{n+}]$ profiles of MR_3Bz (A) and MR_6Bz (B) with different metal ions. Mass of resin: 20 mg. Volume: 20 mL. Solvent: deionized water. pH: 5.0.

Open Access Article. Published on 24 March 2025. Downloaded on 2/10/2026 6:33:01 PM. This article is licensed under a Creative Commons Attribution-NonCommercial 3.0 Unported Licence.

Table 2 Performance parameters for the Pb^{2+} removal process using the MR_nBz resins

Resin	Dose (mg)	Removal (%)	$[Pb^{2+}]_o$ (mg L^{-1})	$[Pb^{2+}]_f$ (mg L^{-1})	Q_e (mg Pb^{2+} per g)	Q_e (mmol Pb^{2+} per g)
MR_2Bz	10	96	28.2	1.13	27.1 ± 1.02	0.131 ± 0.005
MR_3Bz	10	97	28.2	0.84	27.4 ± 0.79	0.132 ± 0.004
MR_4Bz	10	83	28.2	4.79	23.4 ± 1.33	0.113 ± 0.006
MR_6Bz	10	93	28.2	1.97	26.2 ± 2.37	0.126 ± 0.011
MR_8Bz	10	93	28.2	1.97	26.2 ± 1.17	0.126 ± 0.006

Table 3 Performance parameters of the M^{2+} mixture adsorption process using MR_nBz resins

Resin	Optimal dose	M^{n+}	Removal (%)	Q_e (mg M^{n+} per g)	Q_e (mmol M^{n+} per g)	Molar ratio
MR_2Bz	20 mg	Pb^{2+}	91 ± 0.26	17.6	0.11	67 : 18 : 15[a]
		Cd^{2+}	18 ± 0.51			
		Ni^{2+}	12 ± 0.63			
MR_3Bz	20 mg	Pb^{2+}	85 ± 4.92	17.2	0.10	67 : 16 : 17[a]
		Cd^{2+}	17 ± 0.72			
		Ni^{2+}	9 ± 0.29			
MR_4Bz	50 mg	Pb^{2+}	67 ± 6.84	5.8	0.04	58 : 19 : 23[a]
		Cd^{2+}	19 ± 0.12			
		Ni^{2+}	11 ± 0.41			
MR_6Bz	30 mg	Pb^{2+}	90 ± 0.12	11.4	0.07	70 : 30[b]
		Cu^{2+}	15 ± 2.06			
MR_8Bz	20 mg	Pb^{2+}	91 ± 0.13	16.0	0.09	86 : 14[b]
		Cu^{2+}	6 ± 0.67			

[a] Molar ratio Pb^{2+} : Cd^{2+} : Ni^{2+}. [b] Molar ratio Pb^{2+} : Cu^{2+}.

due to the higher amount of cation that is adsorbed. At a lower pH, the ligand is in the neutral form, which decreases the chelating capacity of the resins. At higher values, other lead species such as $PbOH^+$ are formed and no longer complex with the ligand (Fig. S33†). However, the partial adsorption of Pb^{2+} at lower pH may indicate that the physical adsorption mechanism could also be involved, in addition to chemisorption by complexation with the ligand.[59,60]

Having already obtained the optimal resin mass and pH, it was proceeded with the optimization of the contact time, evaluating the adsorption of Pb^{2+} in the **MR_3Bz** and **MR_6Bz** resins from 5 to 360 min. Fig. S34† shows that the **MR_3Bz** resin reached 70% adsorption at 5 min of contact and 96% at 60 min, while the **MR_6Bz** resin presented 62% adsorption at 5 min and reached 100% at 60 min of contact. Based on these results, a contact time of 60 min was established in subsequent experiments.

Another factor which influences the Pb^{2+} adsorption on the resin is the initial concentration of the metal ion. Then, the adsorption of **MR_3Bz**, **MR_4Bz** and **MR_6Bz** resins was evaluated by varying the initial concentration of Pb^{2+} in the solution from 3.5 to 422.6 mg L^{-1}, as shown in Fig. 9 and Tables S1–S3.† The adsorption of Pb^{2+} at the equilibrium Q_e was calculated with eqn (2), and the isotherms show that **MR_3Bz** and **MR_6Bz** reached saturation at 164 mg L^{-1} of Pb^{2+}, while **MR_4Bz** reached saturation at 239 mg L^{-1}. The experimental maximum adsorption (Q_{max}) of Pb^{2+} on **MR_3Bz**, **MR_4Bz** and **MR_6Bz** are 67.1, 44.6 and 74.8 mg Pb^{2+} per g or 0.324, 0.215 and 0.361 mmol Pb^{2+} per g, respectively. It is noteworthy that resins **MR_3Bz** and **MR_6Bz** display removal efficiencies higher than 90% in the concentration interval of 3.5 to 74 mg Pb^{2+} per L, which would allow their use in the treatment of contaminated water with low and high concentrations of Pb^{2+} (Tables S1–S3†).

The Q_e data were fitted using a linearized form of the Langmuir, Freundlich, Temkin and Dubinin–Radushkevich isotherm models (Table S4, eqn (S1)–(S6)†) to determine different parameters that describe the adsorption properties of the **MR_nBz** resins (Tables S5–S7†).[61] The Langmuir model states that there is only a layer of absorbate, a uniform adsorbent surface, and there are no interactions between the adsorbed ions. The Langmuir isotherm non-linear model shows an increase in the adsorption capacity as the initial concentration of the adsorbate increases. The separation factor (R_L) indicates the nature of the adsorption process, such as linear ($R_L = 1$), irreversible ($R_L = 0$), unfavorable ($R_L > 1$), or favorable ($0 < R_L < 1$). The surface coating (θ) represents the fraction of sites occupied by the dissolved adsorbate in the adsorbent. The Freundlich isotherm model proposes that the adsorption process occurs on an inhomogeneous surface, while in the Dubinin–Radushkevich (D–R) isotherm model, no fixed adsorption potential or homogeneous adsorbent surface is considered. This model can be applied to both homogeneous and inhomogeneous surfaces. Finally, in the Temkin isotherm model, the increase in the thickness of the absorbable coating layer on the adsorbent surface causes an increase in the heat adsorption (bT) of all the molecules on the adsorbed layer.[62]

Based on the results of the Langmuir model, the K_L values indicate that Pb^{2+} adsorption is approximately ten times

 © 2025 The Author(s). Published by the Royal Society of Chemistry

Open Access Article. Published on 24 March 2025. Downloaded on 2/10/2026 6:33:01 PM.
This article is licensed under a Creative Commons Attribution-NonCommercial 3.0 Unported Licence.

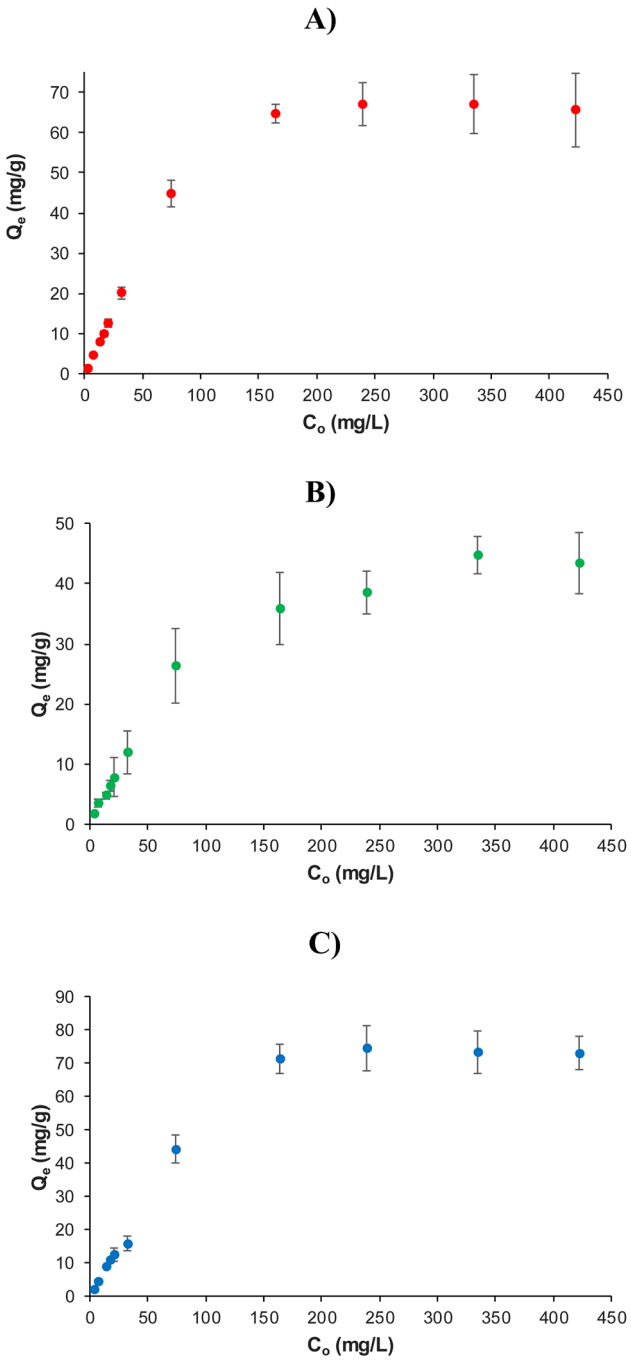

Fig. 9 Non-linear adsorption isotherms of Pb^{2+} in (A) **MR$_3$Bz**, (B) **MR$_4$Bz** and (C) **MR$_6$Bz** resins. Mass of resin: 10 mg. Volume: 10 mL. Solvent: water. pH: 5.0.

stronger in the **MR$_3$Bz** resin than in **MR$_4$Bz** and **MR$_6$Bz**. The separation factor R_L of the three resins is in the range of 0 to 1, which indicates that the adsorption process is favorable in the three resins. Furthermore, the decrease in R_L with increasing concentration indicates that the interaction becomes stronger with increasing Pb^{2+} concentration, and values close to zero indicate that the adsorption is irreversible and extremely strong, particularly in **MR$_3$Bz** (Fig. S35†). The surface coating θ values indicate a gradual increase in the occupation of complexation sites in **MR$_4$Bz** and **MR$_6$Bz** resins as the concentration increases, reaching up to 91% and 94% of occupied sites at the maximum concentration of Pb^{2+}. In the **MR$_3$Bz** resin, the occupation of the sites is more abrupt; that is, an occupation of 95% of the adsorption sites is observed at 32 mg L^{-1} of Pb^{2+} and at the maximum concentration, the occupation is 99.6% (Fig. S36†).

From the Freundlich model, it is observed that the adsorption capacity (K_F) is greater in **MR$_3$Bz**, followed by **MR$_6$Bz**. The inhomogeneity parameters $1/n$, which are also related to the adsorption intensity, indicate that the inhomogeneity is greater in **MR$_3$Bz** and **MR$_6$Bz**; these have the highest Q_e. The parameters of the Temkin model indicate that the Pb^{2+} adsorption process is much more exothermic in the **MR$_3$Bz** resin than in **MR$_6$Bz**, and that it is rather endothermic in the **MR$_3$Bz** resin. The b_T value also indicates that the Pb^{2+} interaction in **MR$_3$Bz** is stronger than that in **MR$_6$Bz**. For its part, the K_T data indicate a greater amount of Pb^{2+} adsorbed on **MR$_6$Bz** compared to the other two resins. The adsorption energy (E_a) values obtained with the D–R model are very low, and indicate that physical adsorption occurs instead of chemical adsorption. However, this point is debatable since, as it is described later, there is a selectivity towards the adsorption of Pb^{2+} in the presence of a molar excess of other cations. This selectivity is given by the chelating properties of the *bCCA* molecules anchored in the resin. Both models, Langmuir and D–R, determine the maximum Pb^{2+} adsorption capacities close to the experimental values. However, considering the R^2 values obtained, the Langmuir model reports the best values with the three resins. So, in general, this model best describes the Pb^{2+} adsorption process in the **MR$_n$Bz** resins (Fig. S37–S39†).[62]

The ΔG^o values for the adsorption of Pb^{2+} in the **MR$_3$Bz**, **MR$_4$Bz** and **MR$_6$Bz** resins were calculated using eqn (3) and (4):[61]

$$K_c = \frac{Q_e}{C_e} \quad (3)$$

$$\Delta G^0 = -RT \ln K_c \quad (4)$$

The **MR$_3$Bz** resin has negative ΔG^0 values in the Pb^{2+} concentration interval of 7.7 to 74 mg L^{-1} with a minimum value of −7.54 kJ mol^{-1} at 20.5 mg L^{-1}. From 164 mg L^{-1}, the values are positive (Table S4†). The **MR$_4$Bz** resin has negative ΔG^0 at the two lowest concentrations, 3.5 and 7.7 mg L^{-1} (−1.54 and −1.08, respectively). From 14.0 mg L^{-1}, the ΔG^0 values are positive (Table S5†). For its part, the **MR$_6$Bz** resin presents negative ΔG^0 values in the range of 3.5 to 164 mg L^{-1} with a minimum value of −8.91 kJ mol^{-1} at 16.9 mg L^{-1}. These results show that at low concentrations, the adsorption process is spontaneous, but significant differences are observed between the resins. In fact, the **MR$_6$Bz** resin is the one with the widest concentration range and the lowest ΔG^0 value compared to the other resins. This difference can be attributed structurally to the length of the spacer that joins the chelating molecule to the polymer matrix.

Subsequently, the adsorption–desorption cycles of the **MR$_3$Bz** and **MR$_6$Bz** resins were performed using 10 mg of resin

© 2025 The Author(s). Published by the Royal Society of Chemistry

Open Access Article. Published on 24 March 2025. Downloaded on 2/10/2026 6:33:01 PM. This article is licensed under a Creative Commons Attribution-NonCommercial 3.0 Unported Licence.

in 10 mL of a Pb^{2+} solution at 290 mg L^{-1} and pH = 5.0. Based on the isotherms, the complexation sites in both resins are saturated at this concentration. The desorption was carried out by washing with 10 mL of a 0.5 M HNO_3 aqueous solution, recovering the resin by filtration. Fig. 10 shows that the **MR_3Bz** resin loses approximately 15% of its adsorption capacity and remains constant until the fourth cycle. However, in the fifth cycle, the adsorption decreases by 40%. The **MR_6Bz** resin maintained its adsorption capacity in the first two cycles. In the third and fourth cycles, it decreased by 15%. Finally, in the fifth cycle, a drop of 40% was observed. These results indicate that these resins can be reused four times while maintaining their adsorption capacity. This gradual decrease in the adsorption capacity of Pb^{2+} may be attributed to the fact that the metal–ligand interaction is so strong and possibly the presence of unexposed complexation sites, which generates the retention of the Pb^{2+} in the resin.

Finally, the adsorption of a metal ions mixture on these resins was evaluated using 10 mL of a solution containing Ni^{2+} (23.7 mg L^{-1}, 0.4038 mmol L^{-1}), Pb^{2+} (33.5 mg L^{-1}, 0.1616 mmol L^{-1}), Cd^{2+} (21.5 mg L^{-1}, 0.1913 mmol L^{-1}) and Cu^{2+} (27.5 mg L^{-1}, 0.4328 mmol L^{-1}) to determine the selectivity in the adsorption of metal ions. As can be seen, there is a molar excess of the other metal ions with respect to Pb^{2+}. The resins with a short spacer remove Pb^{2+}, Ni^{2+} and Cd^{2+} from the solution (Fig. 11 and S40–S44†), while the resins with a long spacer remove Pb^{2+} and Cu^{2+} and no other cation. Independent of the spacer length, all resins predominantly remove Pb^{2+}, despite there being a molar excess of the other cations in the solution. The affinity or selectivity in these resins is consistent with the selectivity if the ***b*BzCCA** ligand towards Pb^{2+}.[50,51] Thus, the behavior of the chelating resins confirms the presence of chelating molecules grafted on the polymer.

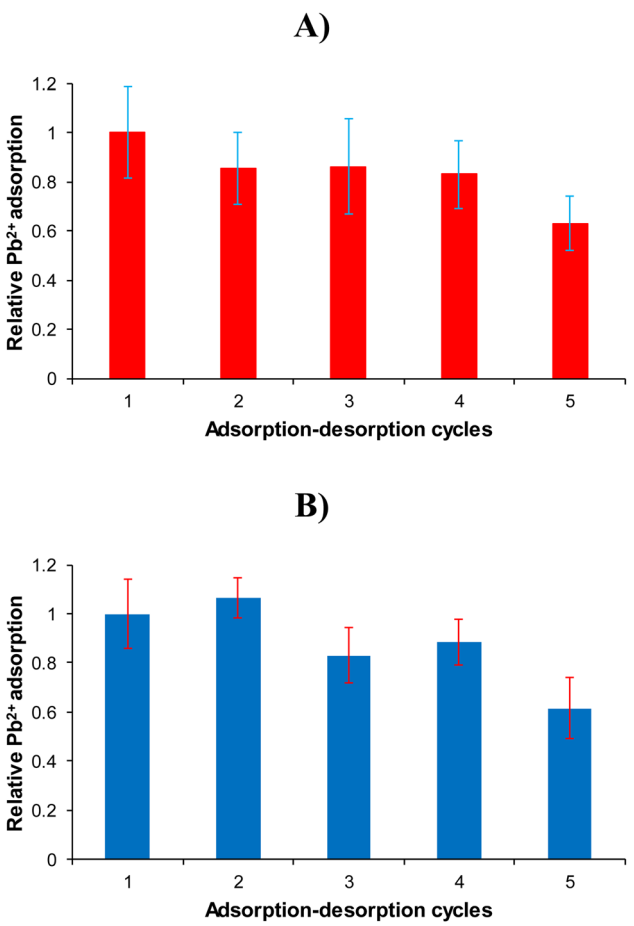

Fig. 10 Relative Pb^{2+} adsorption in several adsorption–desorption cycles for (A) **MR_3Bz** and (B) **MR_6Bz** resins. Mass of resin: 10 mg. Volume: 10 mL. Solvent: water. pH: 5.0.

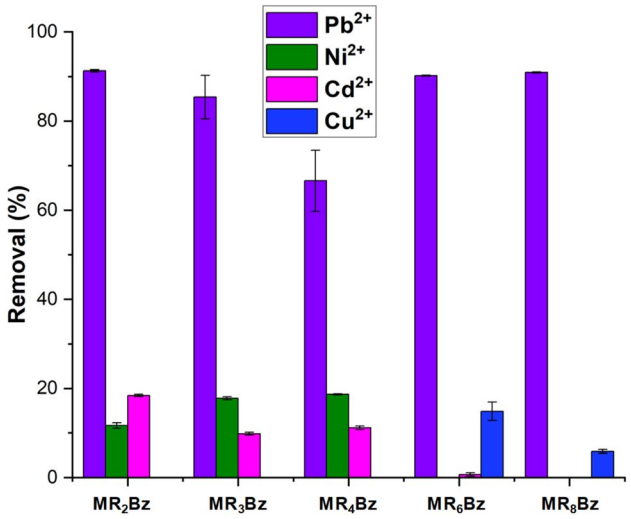

Fig. 11 Metal ion removal percentage of **MR_nBz** resins at their optimal dose. Mass of resin: 10 mg. Volume: 10 mL. Solvent: water. pH: 5.0.

Table 3 shows that the optimal dose required in the removal of a mixture of metal ions increases compared to the exclusive removal of Pb^{2+}, which indicates that metal ions compete for the chelating sites in the resin and a higher amount is required to achieve the maximum removal of cations. As the adsorption capacity depends on the optimal dose, their values are also lower than that obtained in the Pb^{2+} removal experiment. At their optimal doses, the absorption capacity of these resins is in the range of 5.8 to 17.2 mg of M^{2+}/g or 0.04 to 0.11 mmol of M^{2+}/g of resin. The removal% and adsorption are different in each resin, and the molar ratios indicate a greater adsorption of Pb^{2+} compared to the other metal ions. However, the short spacer resins exhibit significant adsorption of Cd^{2+} and Ni^{2+}. The chelating resins with larger spacer **MR_6Bz** and **MR_8Bz** achieved the removal of Pb^{2+} (90% and 91%, respectively) and Cu^{2+}(15% and 6%, respectively) and no other metal ion, showing the effect of the spacer length over the removal capacity and selectivity. Interestingly, the ζ analysis of these resins predicted or indicated the selectivity in the adsorption capacity of these resins.

3.5 Analysis of chelating resins after the metal ion adsorption process

Once chelating resins were used to adsorb metal ions from aqueous solutions, they were dried and characterized by the different available techniques to evaluate the loading of the

© 2025 The Author(s). Published by the Royal Society of Chemistry

Open Access Article. Published on 24 March 2025. Downloaded on 2/10/2026 6:33:01 PM.
This article is licensed under a Creative Commons Attribution-NonCommercial 3.0 Unported Licence.

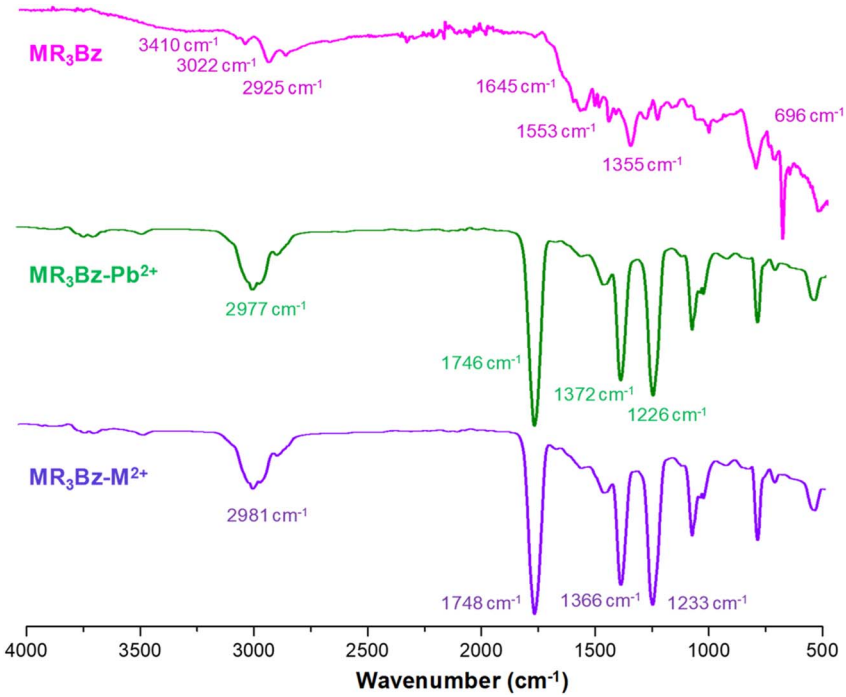

Fig. 12 FTIR spectra of pristine MR_3Bz (magenta), Pb^{2+}-loaded MR_3Bz (green) and M^{2+}-loaded MR_3Bz (purple) resins obtained under a N_2 atmosphere. M^{2+} denotes a mixture of divalent cations.

metal ions. The FTIR spectra of the metal-loaded **MR_3Bz** resins are shown in Fig. 12 and in S45† for **MR_6Bz**. Significant changes are observed in the vibrations; the wide band corresponding to the O–H vibration disappears, and a strong vibration for carbonyls is observed at higher frequency (~1740 cm^{-1}) compared to the pristine resin (~1645 cm^{-1}). Previous reports have indicated that the complexation of carbamoylcarboxylic acids with metal ions such Cu^{2+} and Hg^{2+} causes the O–H vibration to disappear because a carboxylate is formed and changes the energy of the carbonyl vibrations due to both amide and carboxylate groups being coordinated to the metal ion.[48,49]

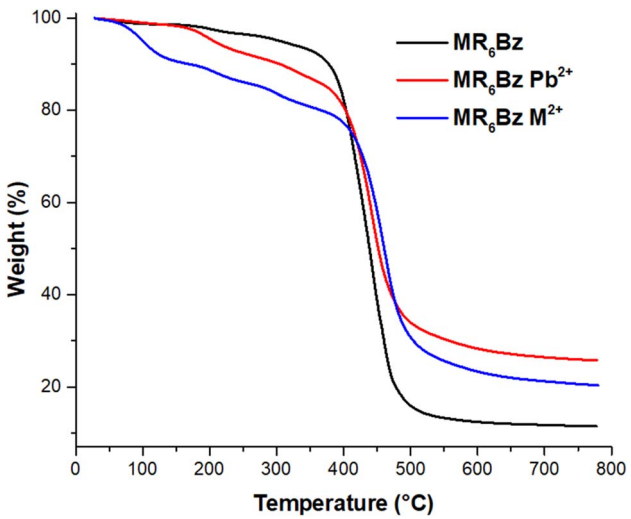

Fig. 13 Thermograms of pristine MR_6Bz resin (black), Pb^{2+}-loaded MR_6Bz (red) and M^{2+}-loaded MR_6Bz (blue) obtained under a N_2 atmosphere. M^{2+} denotes a mixture of divalent cations.

The thermogravimetric analysis of metal-loaded chelating **MR_nBz** resins (Fig. 13 and S46–S49†) shows changes in the thermal decomposition pattern and thermal stability. For the **MR_6Bz** resin, a weight loss stage is observed at around 100 °C, which may correspond to the loss of water adsorbed in the resin or coordinated to the metal complex. Also, the degradation temperature of the polymer increases at around 10 °C, and the percentage of refractory residue increases because of the loading of the metallic components.

Fig. 14 shows the FESEM images at a different scale of M^{2+}-loaded **MR_3Bz** and **MR_6Bz** resins isolated after the adsorption process with a metal ions mixture solution at low concentration. Here, it can be seen that the resin microspheres preserve their size and shape but they are semi-covered by a crust or shell of a different material, which contrasts with the resin surface. The elemental analysis on the surface for the M^{2+}-loaded **MR_3Bz** and **MR_6Bz** resins by EDS shows a high atomic% for carbon and oxygen. Meanwhile, for cadmium, copper, lead and nickel, the atomic% is lower but there is evidence of the presence of these metal ions on the surface (Fig. S50 and S51†). These results evidence the loading of the metallic salts on the resins.

The morphology of the Pb^{2+}-loaded **MR_3Bz** and **MR_6Bz** resins obtained in the isotherm experiments at the highest concentration of Pb^{2+} was observed by FESEM (Fig. 15). The **MR_3Bz** (A and B) and **MR_6Bz** (C and D) resins preserve their spherical shape and size, but their surface is completely covered by the shell of a different material and the surface looks very rough. The elemental analysis by EDS for the Pb^{2+}-loaded resins

© 2025 The Author(s). Published by the Royal Society of Chemistry

Open Access Article. Published on 24 March 2025. Downloaded on 2/10/2026 6:33:01 PM.
This article is licensed under a Creative Commons Attribution-NonCommercial 3.0 Unported Licence.

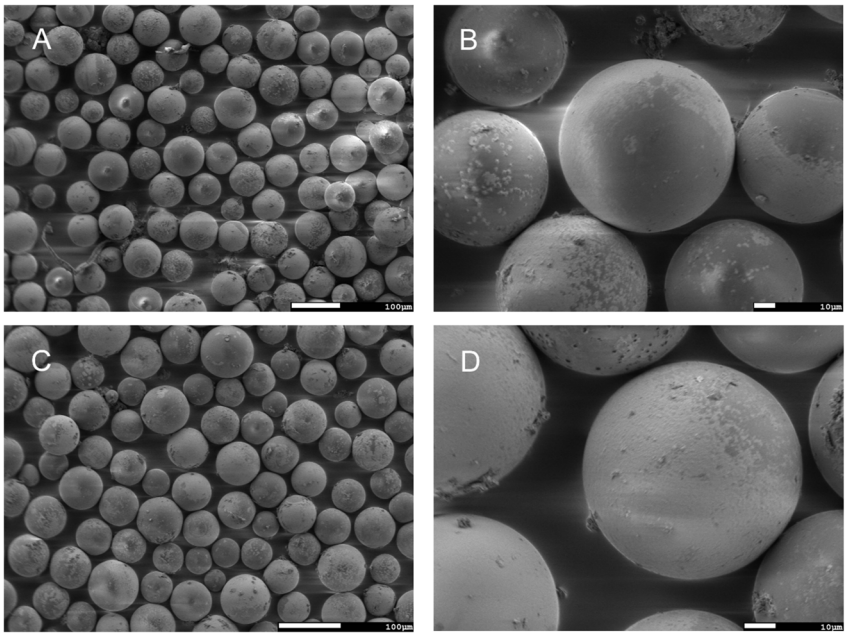

Fig. 14 FESEM images of M^{2+}-loaded **MR_3Bz** (A and B) and **MR_6Bz** (C and D) resins.

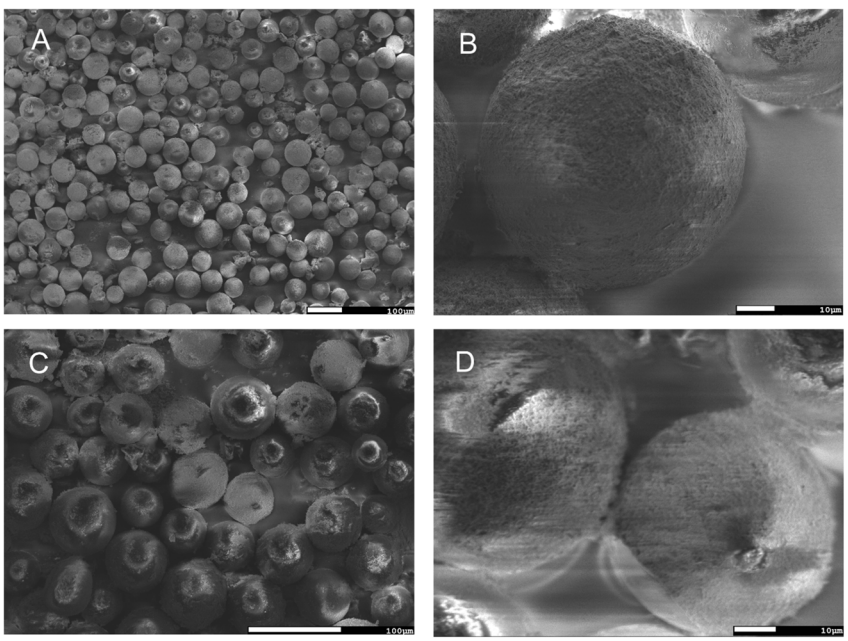

Fig. 15 FESEM images of Pb^{2+}-loaded **MR_3Bz** (A and B) and **MR_6Bz** (C and D) resins.

obtained after the treatment of Pb^{2+} solutions at low and high concentrations shows that the atomic% of lead on the surface increases considerably as the initial concentration in the solution increases. The resins immersed into a Pb^{2+} solution at 28 mg L^{-1} show 0.16 and 1.74 atomic% of lead, respectively (Fig S52 and S53†), while those immersed into a solution at 340 mg L^{-1} show 27.86 and 29.77 atomic% of lead, respectively (Fig. S54 and S55†). These results are consistent with the adsorption ratios found in lead adsorption experiments on these resins at low and high concentrations of the metal ion.

3.6 Comparison of the adsorption performance of MR_nBz resins with other chelating resins

The literature describes the performance of several functionalized Merrifield's resins with different ligands in the removal of metal ions showing different adsorption capacities. Table 4 shows the adsorption capacity of several **MR**-chelating resins, indicating the initial concentration of metal ions, volume of treated water, amount of resin and the experimental method (batch or packed column). The adsorption efficiency of the **MR_nBz** chelating resins developed in this work is slightly lower

© 2025 The Author(s). Published by the Royal Society of Chemistry

Open Access Article. Published on 24 March 2025. Downloaded on 2/10/2026 6:33:01 PM. This article is licensed under a Creative Commons Attribution-NonCommercial 3.0 Unported Licence.

Table 4 Comparison of the adsorption capacity of various MR-functionalized adsorbents for heavy metal ions

Adsorbent	Adsorption capacity (mmol g^{-1})	Method	Reference
CPS-DI	1.35 (Pb^{2+}), 0.94 (Ni^{2+}), 2.55 (Cu^{2+})	Batch, 250 rpm, 0.1 g/0.1 L (100 ppm)	34
Thiourea calixarene	84.80 (Pb^{2+})	Batch, 160 rpm, 0.1 g/0.01 L (5×10^{-5} $M \approx$ 10.4 ppm)	37
Piperidine calixarene	2.1 (Cr^{6+})	Batch, 0.025 g/0.02 L (1×10^{-4} $M \approx$ 5.2 ppm)	38
CMPDB	0.21 (Cr^{6+})	Batch, 1.0 g/0.1 L (100 ppm)	39
MR-Q	1.65 (Pb^{2+})	Batch, 0.01 g/0.02 L (350 ppm)	41
MR_6Q	1.21 (Pb^{2+})	Column, 0.04 g/1.0 mL min^{-1} (0.11 ppm)	42
CPS-TA	1.11 (Pb^{2+}), 2.97 (Ni^{2+}), 4.23 (Cu^{2+})	Batch, 0.1 g/0.1 L (100 ppm)	43
Thiacalixarene	5.5 (Eu^{3+})	Batch, 0.1 g/0.02 L (10 ppm)	44
PVT-*g*-PS	1.52 (Pb^{2+}), 2.65 (Cu^{2+}), 3.36 (Cr^{6+})	Batch, 0.1 g/0.1 L (4 mM)	45
PS-CS	0.14 (Cu^{2+})	Batch, 0.0135 g/0.1 L (10 ppm)	46
ASA/IMEA-PGMA@PS	1.57 (Pb^{2+}), 0.70 (Cd^{2+}), 0.87 (Cu^{2+}), 1.19 (Cr^{6+})	Batch, 0.1 g/0.025 L (4.0 mM)	47
MR_nBz	0.11 to 0.13 (Pb^{2+})	Batch, 0.01 g/0.01 L (28 ppm)	This work
MR_3Bz	0.322 (Pb^{2+})	Batch, 0.01 g/0.01 L (164 ppm)	This work
MR_6Bz	0.392 (Pb^{2+})	Batch, 0.01 g/0.01 L (164 ppm)	This work
MR_2Bz	0.10–0.11 (Pb^{2+}, Cd^{2+} and Ni^{2+} mixture)	Batch, 0.02 g/0.01 L (33.5 ppm, 21.5 ppm, 24.7 ppm)	This work
MR_3Bz			
MR_8Bz	0.09 (Pb^{2+} and Cu^{2+} mixture)	Batch, 0.02 g/0.01 L (33.5 ppm, and 27.5 ppm)	This work

compared to other materials. This difference in the adsorption capacity is directly related to the loading of the resin, the affinity of the chelating molecule incorporated into the polymer matrix, and also with the expansion capacity in the aqueous medium, since the expansion allows the diffusion of the metal cation towards the matrix. Also, the design of the experiment, batch or column, influences the adsorption. However, there are some main aspects that distinguishes the performance of the **MR_nBz** resins: (1) the chelating molecules attached to the resins have low structural complexity, facilitating their preparation at large scale; (2) they works well in the adsorption of metal ions present in water at low and high concentration. Meanwhile, in some of the listed resins, the initial concentration of metals is high (100 and 350 ppm); (3) their performance was successful in the individual removal of Pb^{2+} ion, and in the removal of a mixture of metal ions (Pb^{2+} and Cu^{2+} or Pb^{2+}, Cd^{2+} and Ni^{2+}), showing a significant adsorption and selectivity towards Pb^{2+} ions. The previous reported resins were evaluated for individual metal ions, and do not include results for a mixture of metal ions.

4. Conclusions

The functionalization of Merrifield's resin with chelating *bCCA* molecules provides specificity to the ion adsorption capacity of this material. The functionality and spacer length influence the adsorption capacity and selectivity. **MR_nBz** resins display a predominant or selective Pb^{2+} adsorption. However, the spacer length plays an important role in the adsorption of other metal ions. Short spacers improve the adsorption of Cd^{2+} and Ni^{2+}, while larger spacers favor the adsorption of Cu^{2+}. Based on the adsorption capacity and the parameters of the isotherm models that describe the adsorption properties, it was possible to select the **MR_3Bz** resin as the best among this mini-library of chelating resins, although they all have good characteristics. The adsorption properties of these resins are comparable with other reported resins considering the conditions used in these experiments. On the other hand, FTIR and TGA analyses demonstrated the functionalization of the Merrifield's resin in each synthetic step, as well as M^{2+}-loading in the resin after the adsorption process. FESEM images provide unequivocal evidence of the loading of metallic materials on the resin surface and the preservation of its structure along the synthesis steps and after the removal process. Finally, the ζ analysis of these resins indicated the selectivity in the adsorption capacity. Currently, we are conducting further research to support the use of Merrifield's resin and other *bCCA* molecules having aniline, pyridine or carboxylic substituents on the amide, with the aim to improve its adsorption capacity and/or to modulate it towards the adsorption of different cations.

Data availability

The data supporting this article have been included as part of the ESI.†

Conflicts of interest

There are no conflicts to declare.

Acknowledgements

The authors gratefully acknowledge Tecnológico Nacional de México (TECNM) for supporting this research study through the research project "Evaluación de resinas quelantes funcionalizadas con ácidos carbamoilcarboxílicos en el tratamiento de aguas contaminadas con metales" (Grant No. 13763.22-P). José García-Elías is also thankful to CONAHCYT for the scholarship granted to carry out his doctoral studies.

References

1 N. A. A. Qasem, R. H. Mohammed and D. U. Lawal, Removal of heavy metal ions from wastewater: a comprehensive and critical review, *npj Clean Water*, 2021, **4**, 36, DOI: **10.1038/s41545-021-00127-0**.

Open Access Article. Published on 24 March 2025. Downloaded on 2/10/2026 6:33:01 PM. This article is licensed under a Creative Commons Attribution-NonCommercial 3.0 Unported Licence.

2 A. Pratush, A. Kumar and Z. Hu, Adverse effect of heavy metals (As, Pb, Hg, and Cr) on health and their bioremediation strategies: a review, *Int. Microbiol.*, 2018, **21**, 97–106, DOI: 10.1007/s10123-018-0012-3.

3 Z. Rahman and V. P. Singh, The relative impact of toxic heavy metals (THMs) (arsenic (As), cadmium (Cd), chromium (Cr)(VI), mercury (Hg), and lead (Pb)) on the total environment: an overview, *Environ. Monit. Assess.*, 2019, **191**, 419, DOI: 10.1007/s10661-019-7528-7.

4 United States Environmental Protection Agency. *EPA, Office of Water, 2012 Edition of the Drinking Water Standards and Health Advisories (EPA 822-S-12-001)*, Spring, 2012.

5 S. J. Hawkes, What Is a "Heavy Metal", *J. Chem. Educ.*, 1997, **74**, 1374, DOI: 10.1021/ed074p1374.

6 J. Miller, What Makes Heavy Metal "Heavy", *J. Aesthet. Art Critic.*, 2022, **80**, 70–82, DOI: 10.1093/jaac/kpab065.

7 Z. Li, H. Kuang, L. Li, M. Wu, Z. Liao, K. Zeng, Y. Ye and R. Fan, What adverse health effects will environmental heavy metal co-exposure bring us: based on a biological monitoring study of sanitation workers, *Environ. Sci. Pollut. Res.*, 2023, **30**, 35769–35780, DOI: 10.1007/s11356-022-24805-9.

8 NORMA Oficial Mexicana NOM-001-SEMARNAT-2021, *Que establece los límites permisibles de contaminantes en las descargas de aguas residuales en cuerpos receptores propiedad de la nación*, Diario Oficial de la Federación de la Secretaría de Gobernación, 2022.

9 T. A. Kurniawan, G. Y. S. Chan, W. H. Lo and S. Babel, Physico-chemical treatment techniques for wastewater laden with heavy metals, *Chem. Eng. J.*, 2006, **118**, 83–98, DOI: 10.1016/j.cej.2006.01.015.

10 K. A. Momina, Feasibility of the adsorption as a process for its large scale adoption across industries for the treatment of wastewater: Research gaps and economic assessment, *J. Cleaner Prod.*, 2023, **388**, 136014, DOI: 10.1016/j.jclepro.2023.136014.

11 Z. Raji, A. Karim, A. Karam and S. Khalloufi, Adsorption of heavy metals: mechanisms, kinetics, and applications of various adsorbents in wastewater remediation—A review, *Waste*, 2023, **1**, 775–805, DOI: 10.3390/waste1030046.

12 A. M. Elgarahy, M. G. Eloffy, E. Guibal, H. M. Alghamdi and K. Z. Elwakeel, Use of biopolymers in wastewater treatment: A brief review of current trends and prospects, *Chin. J. Chem. Eng.*, 2023, **64**, 292–320, DOI: 10.1016/j.cjche.2023.05.018.

13 A. M. Elgarahy, A. Maged, M. G. Eloffy, M. Zahran, S. Kharbish, K. Z. Elwakeel and A. Bhatnagar, Geopolymers as sustainable eco-friendly materials: Classification, synthesis routes, and applications in wastewater treatment, *Sep. Purif. Technol.*, 2023, **324**, 124631, DOI: 10.1016/j.seppur.2023.124631.

14 A. M. Elgarahy, A. S. Al-Bogami, A. Akhdhar, Z. A. Khan and K. Z. Elwakeel, Silver ions immobilized on thiourea/formaldehyde resin for solid phase extraction of iodide ions from aqueous solution, *J. Mol. Liq.*, 2023, **376**, 121474, DOI: 10.1016/j.molliq.2023.121474.

15 K. Z. Elwakeel, M. M. Ahmed, A. Akhdhar, M. G. M. Sulaiman and Z. A. Khan, Recent advances in alginate-based adsorbents for heavy metal retention from water: a review, *Desalin. Water Treat.*, 2022, **272**, 50–74, DOI: 10.5004/dwt.2022.28834.

16 A. Benettayeb, A. Morsli, K. Z. Elwakeel, M. F. Hamza and E. Guibal, Recovery of Heavy Metal Ions Using Magnetic Glycine-Modified Chitosan—Application to Aqueous Solutions and Tailing Leachate, *Appl. Sci.*, 2021, **11**(18), 8377, DOI: 10.3390/app11188377.

17 K. Z. Elwakeel, M. F. Hamza and E. Guibal, Effect of agitation mode (mechanical, ultrasound and microwave) on uranium sorption using amine- and dithizone-functionalized magnetic chitosan hybrid materials, *Chem. Eng. J.*, 2021, **411**, 128553, DOI: 10.1016/j.cej.2021.128553.

18 K. Z. Elwakeel, A. S. Al-Bogami and E. Guibal, 2-Mercaptobenzimidazole derivative of chitosan for silver sorption – Contribution of magnetite incorporation and sonication effects on enhanced metal recovery, *Chem. Eng. J.*, 2021, **403**, 12626, DOI: 10.1016/j.cej.2020.126265.

19 K. Z. Elwakeel, A. Shahat, Z. A. Khan, W. Alshitari and E. Guibal, Magnetic metal oxide-organic framework material for ultrasonic-assisted sorption of titan yellow and rose bengal from aqueous solutions, *Chem. Eng. J.*, 2020, **392**, 123635, DOI: 10.1016/j.cej.2019.123635.

20 V. Beaugeard, J. Muller, A. Graillot, X. Ding, J. J. Robin and S. Monge, Acidic polymeric sorbents for the removal of metallic pollution in water: A review, *React. Funct. Polym.*, 2020, **152**, 104599, DOI: 10.1016/j.reactfunctpolym.2020.104599.

21 R. B. Merrifield, Solid Phase Peptide Synthesis. I. The Synthesis of a Tetrapeptide, *J. Am. Chem. Soc.*, 1963, **85**, 2149–2154, DOI: 10.1021/ja00897a025.

22 F. Dumeignil, J. F. Paul and S. Paul, Heterogeneous Catalysis with Renewed Attention: Principles, Theories, and Concepts, *J. Chem. Educ.*, 2017, **94**, 675–689, DOI: 10.1021/acs.jchemed.6b00611.

23 L. Gao, K. Deng, J. Zheng, B. Liu and Z. Zhang, Efficient oxidation of biomass derived 5-hydroxymethylfurfural into 2,5-furandicarboxylic acid catalyzed by Merrifield resin supported cobalt porphyrin, *Chem. Eng. J.*, 2015, **270**, 444–449, DOI: 10.1016/j.cej.2015.02.068.

24 S. N. Jadhav, A. S. Kumbhar, S. S. Mali, C. K. Hong and R. S. Salunkhe, A Merrifield resin supported Pd-NHC complex with a spacer(Pd-NHC@SP-PS) for the Sonogashira coupling reaction under copper- and solvent-free conditions, *New J. Chem.*, 2015, **39**, 2333–2341, DOI: 10.1039/c4nj02025a.

25 L. Pastor-Pérez, C. Lloret-Fernández, H. Anane, M. L. El Idrissi Moubtassim, M. Julve and S. E. Stiriba, An approach to polymer-supported triplet benzophenone photocatalysts. Application to sustainable photocatalysis of an α-diazocarbonyl compound, *RSC Adv.*, 2013, **3**, 25652–25656, DOI: 10.1039/c3ra45321a.

26 M. Fantinel, N. Valiati, P. A. M. Moro and M. M. Sá, Amino-modified Merrifield resins as recyclable catalysts for the safe and sustainable preparation of functionalized α-diazo carbonyl compounds, *Tetrahedron*, 2021, **86**, 132081, DOI: 10.1016/j.tet.2021.

© 2025 The Author(s). Published by the Royal Society of Chemistry

Open Access Article. Published on 24 March 2025. Downloaded on 2/10/2026 6:33:01 PM. This article is licensed under a Creative Commons Attribution-NonCommercial 3.0 Unported Licence.

27 J. Li, G. Yang, Y. Qin, X. Yang and Y. Cui, Recyclable Merrifield resin-supported thiourea organocatalysts derived from L-proline for direct asymmetric aldol reaction, *Tetrahedron:Asymmetry*, 2011, **22**, 613–618, DOI: 10.1016/j.tetasy.2011.03.016.

28 P. Basu, T. K. Dey, A. Ghosh, S. Biswas, A. Khan and S. M. Islam, An efficient one-pot synthesis of industrially valuable primary organic carbamates and: N -substituted ureas by a reusable Merrifield anchored iron(II)-anthra catalyst [Fe^{II}(Anthra-Merf)] using urea as a sustainable carbonylation source, *New J. Chem.*, 2020, **44**, 2630–2643, DOI: 10.1039/c9nj05675k.

29 M. Aguilar-Martínez, J. T. Vargas-Durazo, A. Ochoa-Terán, H. Santacruz-Ortega, K. Ochoa-Lara, A. Zizumbo-López and J. C. Gálvez-Ruíz, Neutral reducing agents supported on Merrifield resin obtained by solid phase organic synthesis, *Tetrahedron*, 2021, **91**, 132195, DOI: 10.1016/j.tet.2021.132195.

30 S. Adeyeye Nafiu, A. M. Ajeebi, H. S. Alghamdi, M. A. Aziz and M. Nasiruzzaman Shaikh, Solid-Supported Catalysts for Organic Functional Group Transformations, *Asian J. Org. Chem.*, 2023, **12**, e202300051, DOI: 10.1002/ajoc.202300051.

31 G. Pina-Luis, G. A. Rosquete Pina, A. C. Valdés González, A. Ochoa-Terán, I. Rivero-Espejel and M. E. Díaz-García, Morin functionalized Merrifield's resin: A new material for enrichment and sensing heavy metals, *React. Funct. Polym.*, 2012, **72**, 61–68, DOI: 10.1016/j.reactfunctpolym.2011.10.003.

32 H. J. Lee, K. I. Lee, M. Kim, Y. W. Suh, H. S. Kim and H. Lee, Diamine-anchored polystyrene resins for reversible SO2 adsorption, *ACS Sustainable Chem. Eng.*, 2016, **4**, 2012–2019, DOI: 10.1021/acssuschemeng.5b01325.

33 X. Yu, J. Hao, Z. Xi, T. Liu, Y. Lin and B. Xu, Investigation of low concentration SO2 adsorption performance on different amine-modified Merrifield resins, *Atmos. Pollut. Res.*, 2019, **10**, 404–411, DOI: 10.1016/j.apr.2018.08.015.

34 B. Zou, S. Zhang, P. Sun, Z. Ye, Q. Zhao, W. Zhang and L. Zhou, Preparation of a novel Poly-chloromethyl styrene chelating resin containing heterofluorenone pendant groups for the removal of Cu (II), Pb (II), and Ni (II) from wastewaters, *Colloids Interface Sci. Commun.*, 2021, **40**, 100349, DOI: 10.1016/j.colcom.2020.100349.

35 B. Zou, S. Zhang, P. Sun, Q. Zhao, W. Zhang, X. Zhang, *et al.*, Synthesis of a novel Poly-chloromethyl styrene chelating resin containing Tri-pyridine aniline groups and its efficient adsorption of heavy metal ions and catalytic degradation of bisphenol A, *Sep. Purif. Technol.*, 2021, **275**, 119234, DOI: 10.1016/j.seppur.2021.119234.

36 R. S. Praveen, G. R. K. Naidu and T. Prasada Rao, Dithiocarbamate functionalized or surface sorbed Merrifield's resin beads as column materials for on line flow injection-flame atomic absorption spectrometry determination of lead, *Anal. Chim. Acta*, 2007, **600**, 205–213, DOI: 10.1016/j.aca.2007.01.012.

37 A. Ali-Bhatti, A. Ali-Bhatti, I. Bakhsh-Solangi and S. Memon, Pb^{2+} adsorption behavior of calix[4]arene based Merrifield Resin, Desalination and Water, *Tratment*, 2013, **51**, 4666–4674, DOI: 10.1080/19443994.2013.769757.

38 A. Ezgi, M. Yilmaz and R. A. Bartsch, Immobilization of cyclic alkylamine calix[4]arene derivatives on Merrifield resin evaluation of extraction ability toward dichromate, *J. Macromol. Sci.*, 2006, **43**, 477–486, DOI: 10.1080/10601320600575140.

39 V. K. Jean, R. A. Pandya, S. G. Pillai, P. S. Shrivastav and Y. K. Agrawal, Merrifield resin supported chelate forming calix[4]arene-o-vanillinthiosemicarbazone resin employed for separation, preconcentration and trace determination of Cr(IV), As(III) and Ti(I) in water samples, *Sep. Sci. Technol.*, 2006, **41**, 123–147, DOI: 10.1080/01496390500445626.

40 S. Pramanik, S. Dhara, S. S. Bhattacharyya and P. Chattopadhyay, Separation and determination of some metal ions on new chelating resins containing N,N donor sets, *Anal. Chim. Acta*, 2006, **556**, 430–437, DOI: 10.1016/j.aca.2005.09.065.

41 D. M. Luaces-Alberto, A. C. Valdés-González, C. A. Alonso-Vilches, L. L. Alba-Gutierrez, S. Fernandez-Puig and A. M. Gutiérrez-Carreras, Inmovilización de quercetina sobre resina de Merrifield mediante síntesis orgánica en fase sólida asistida por microondas. Estudio Preliminar de La Retención de Pb(II), *Rev. Cubana Quim.*, 2017, **29**, 229–242.

42 S. Fernández-Puig, M. D. Luaces-Alberto, V. Vallejo-Becerra, A. Ochoa Terán, A. U. Chávez-Ramírez and A. C. Valdés González, Modified Merrifield's resin materials used in capturing of Pb(II) ions in water, *Mater. Res. Express*, 2019, **6**, 115104, DOI: 10.1088/2053-1591/ab4470.

43 M. S. Lukashova, K. N. Belikov, K. Y. Bryleva, S. G. Kharchenko, S. G. Vishnevsky and V. I. Kalchenko, Merrifield resin modified with thiacalixarene-tetraphosphonates: synthesis, characterization and europium sorption, *Funct. Mater.*, 2016, **23**, 111–119, DOI: 10.15407/fm23.01.111.

44 Y. Chen, M. He, C. Wang and Y. Wei, A novel polyvinyltetrazole-grafted resin with high capacity for adsorption of Pb(II), Cu(II) and Cr(III) ions from aqueous solutions, *J. Mater. Chem. A*, 2014, **2**, 10444–10453, DOI: 10.1039/c4ta01512f.

45 W. Jiang, X. Chen, B. Pan, Q. Zhang, L. Teng, Y. Chen and L. Liu, Spherical polystyrene-supported chitosan thin film of fast kinetics and high capacity for copper removal, *J. Hazard. Mater.*, 2014, **276**, 295–301, DOI: 10.1016/j.jhazmat.2014.05.032.

46 J. Ma, J. Shen, C. Wang and Y. Wei, Preparation of dual-function chelating resin with high capacity and adjustable adsorption selectivity to variety of heavy metal ions, *J. Taiwan Inst. Chem. Eng.*, 2018, **91**, 532–538, DOI: 10.1016/j.jtice.2018.05.038.

47 A. Ochoa-Terán, J. Estrada-Manjarrez, M. Martínez-Quiroz, M. A. Landey-Álvarez, E. Alcántar Zavala, G. Pina-Luis, H. Santacruz Ortega, L. E. Gómez-Pineda, J. Z. Ramírez, D. Chávez, J. Montes Ávila, V. Labastida-Galván and M. Ordoñez, A novel and highly regioselective synthesis of

Open Access Article. Published on 24 March 2025. Downloaded on 2/10/2026 6:33:01 PM. This article is licensed under a Creative Commons Attribution-NonCommercial 3.0 Unported Licence.

new carbamoylcarboxylic acids from dianhydrides, *Sci. World J.*, 2014, **2014**, 725981, DOI: 10.1155/2014/725981.

48 M. Martínez-Quiroz, A. Ochoa-Terán, M. Aguilar-Martínez, J. García-Elías, H. Santacruz Ortega, V. Miranda-Soto and G. Pina-Luis, New fluorescent metal receptors based on 4,4′-carbonyl bis(carbamoylbenzoic) acid analogues with naphthalene fluorophore, *Supramol. Chem.*, 2017, **29**, 477–488, DOI: 10.1080/10610278.2016.1277585.

49 V. Ravindar, S. J. Swamy, S. Srihari and P. Lingaiah, Synthesis and spectral studies of copper(II) complexes with amide group ligands, *Polyhedron*, 1985, **4**, 1511–1518, DOI: 10.1016/S0277-5387(00)86991-0.

50 M. Martínez-Quiroz, E. A. López-Maldonado, A. Ochoa-Terán, M. T. Oropeza-Guzman, G. E. Pina-Luis and J. Zeferino-Ramírez, Innovative uses of carbamoyl benzoic acids in coagulation-flocculation's processes of wastewater, *Chem. Eng. J.*, 2017, **307**, 981–988, DOI: 10.1016/j.cej.2016.09.011.

51 C. U. Montaño-Medina, L. M. López-Martínez, A. Ochoa-Terán, E. A. López-Maldonado, M. I. Salazar-Gastelum, B. Trujillo-Navarrete, S. Pérez-Sicairos and J. M. Cornejo Bravo, New pyridyl and aniline-functionalized carbamoilcarboxylic acids for removal of metal ions from water by coagulation-flocculation process, *Chem. Eng. J.*, 2023, **451**, 138396, DOI: 10.1016/j.cej.2022.138396.

52 M. Martínez-Quiroz, E. A. López-Maldonado, A. Ochoa-Terán, G. E. Pina-Luis and M. T. Oropeza Guzmán, Modification of chitosan with carbamoyl benzoic acids for testing its coagulant-flocculant and binding capacities in removal of metallic ions typically contained in plating wastewater, *Chem. Eng. J.*, 2018, **332**, 749–756, DOI: 10.1016/j.cej.2017.09.042.

53 C. L. Castro-Riquelme, E. A. López-Maldonado, A. Ochoa-Terán, E. Alcántar-Zavala, B. Trujillo-Navarrete, S. Pérez-Sicairos, V. Miranda-Soto and A. Zizumbo-López, Chitosan-carbamoylcarboxylic acid grafted polymers for removal of metal ions in wastewater, *Chem. Eng. J.*, 2023, **426**, 141034, DOI: 10.1016/j.cej.2022.141034.

54 I. Langmuir, The adsorption of gases on plane surfaces of glass, mica and platinum, *J. Am. Chem. Soc.*, 1918, **40**, 1361–1403, DOI: 10.1021/ja02242a004.

55 P. Forns and F. Albericio, Encyclopedia of Reagents for Organic Synthesis, *Merrifield Resin*, 2001. DOI: 10.1002/047084289X.rn00197.

56 W. Mansour, M. Fettouhi, Q. Saleem and B. El Ali, Robust alkyl-bridged bis(*N*-heterocyclic carbene)palladium(II) complexes anchored on Merrifield's resin as active catalysts for the selective synthesis of flavones and alkynones, *Appl. Organomet. Chem.*, 2021, **35**, e6195, DOI: 10.1002/AOC.6195.

57 R. R. da Silva, L. C. de Oliveira, G. V. M. Gabriel, J. I. Soletti, M. D. Bispo, S. S. Paulino, S. M. P. Meneghetti, G. C. de Assis, A. P. Fernandes and W. G. Botero, Interaction of lead and calcium with biochar produced from cassava waste: perspectives for agricultural and environmental application, *J. Braz. Chem. Soc.*, 2022, **33**, 1402–1413, DOI: 10.21577/0103-5053.20220076.

58 T. Yoshida, T. Yamaguchi, Y. Iida and S. Nakayama, XPS study of Pb(II) adsorption on g-Al_2O_3 surface at high pH conditions, *J. Nucl. Sci. Technol.*, 2003, **40**, 672–678, DOI: 10.1080/18811248.2003.9715405.

59 Z. Raji, A. Karim, A. Karam and S. Khalloufi, Adsorption of heavy metals: mechanisms, kinetics, and applications of various adsorbents in wastewater remediation—A review, *Waste*, 2023, **1**, 775–805, DOI: 10.3390/waste1030046.

60 I. T. Kabogo, G. S. Nyamato, J. Ogunah, S. Maqinana and S. O. Ojwach, Extraction of heavy metals from water using chelating agents: a comprehensive review, *Int. J. Environ. Sci. Technol.*, 2024, **21**, 8749–8792, DOI: 10.1007/s13762-024-05586-9.

61 N. Mehrmanda, M. K. Moraveji and A. Parvareh, Adsorption of Pb(II), Cu(II) and Ni(II) ions from aqueous solutions by functionalized henna powder (*Lawsonia inermis*); isotherm, kinetic and thermodynamic studies, *Int. J. Environ. Anal. Chem.*, 2020, **10**, 1–22, DOI: 10.1080/03067319.2020.1715376.

62 X. Chen, Md F. Hossain, C. Duan, J. Lu, Y. F. Tsang, Md S. Islam and Y. Zhou, Isotherm models for adsorption of heavy metals from water - A review, *Chemosphere*, 2022, **307**, 135145, DOI: 10.1016/j.chemosphere.2022.135545.

© 2025 The Author(s). Published by the Royal Society of Chemistry